Ultrastructural Pathology, 2014; 38(2): 116–140

ISSN: 0191-3123 print / 1521-0758 online
DOI: 10.3109/01913123.2013.852645

informa
healthcare

ORIGINAL ARTICLE

Synergistic Antitumor Cytotoxic Actions of Ascorbate and Menadione on Human Prostate (DU145) Cancer Cells In Vitro: Nucleus and Other Injuries Preceding Cell Death by Autoschizis

Jacques Gilloteaux, MSc, EdM, DSc[1], James M. Jamison, PhD[2], Deborah Neal, BS, MT[2], and Jack L. Summers, MD, PhD[2]

[1]*Department of Anatomical Sciences, St Georges' University International School of Medicine, K B Taylor Scholar's Programme, Newcastle upon Tyne, UK and* [2]*The Apatone Development Center, St. Thomas Hospital, Summa Research Foundation, Akron, OH, USA*

ABSTRACT

Scanning (SEM) and transmission electron microscopy (TEM) were used to characterize the cytotoxic effects of ascorbate (VC), menadione (VK_3), or a VC:VK_3 combination on a human prostate carcinoma cell line (DU145) following a 1-h vitamin treatment and a subsequent 24-h incubation in culture medium. Cell alterations examined by light and electron microscopy were treatment-dependent with $VC + VK_3 > VK_3 > VC >$ Sham. Oxidative stress-induced damage was found in most organelles. This report describes injuries in the tumor cell nucleus (chromatin and nucleolus), mitochondria, endomembranes, lysosomal bodies (autophagocytoses) and inclusions. Morphologic alterations suggest that cytoskeleton damage is likely responsible for the superficial cytoplasmic changes, including major changes in cell shape and size and the self-excising phenomena. Unlike apoptotic bodies, the excised pieces contain ribonucleoproteins, but not organelles. These deleterious events cause a progressive, significant reduction in the tumor cell size. During nuclear alterations, the nuclei maintain their envelope during chromatolysis and karyolysis until cell death, while nucleoli undergo a characteristic segregation of their components. In addition, changes in fat and glycogen storage are consistent the cytotoxic and metabolic alterations caused by the respective treatments. All cellular ultrastructural changes are consistent with cell death by autoschizis and not apoptosis or other kinds of cell death.

Keywords: Autoschizis, carcinoma, cell death, DU145, nucleus, organelles, oxidative stress, prostate

Prostate cancer is one of the most frequently diagnosed cancers in males throughout the world [1–3]. In the US or European countries, it is already the second leading cause of cancer-related mortality [3] and its frequency and mortality rate has increased over the past 40 years. Advances in screening and diagnosis have allowed detection of the disease in the early stages and led to the development of therapeutic options that can be curative including surgery and radiation [4,5]. However, for late-stage disseminated disease, current therapies are merely palliative [6]. For example, while androgen ablation (the first line of treatment for patients with prostatic carcinoma) [7] produces a good initial response in 80–90% of patients with metastatic disease, remissions last only 2–3 years and then the patients progress to an androgen-insensitive phase of disease with a worse prognosis. Likewise, chemotherapy, the

Received 19 August 2013; Revised 21 September 2013; Accepted 1 October 2013; Published online 24 January 2014

Correspondence: Prof. Jacques Gilloteaux, Department of Anatomical Sciences, St. George's University International School of Medicine, UNN- Life Sciences, Drill Hall 013, Newcastle upon Tyne NE1 8ST, UK. Tel: 44 (0)191 227 4854/ 4855. Fax: 44 (0) 191 227 4824. E-mail: jgilloteaux@sgu.edu

second line of treatment, produces a subjective, short-term improvement and is not well tolerated by the patients [8]. These shortcomings call attention to a need for developing of an effective and efficient regimen for treating hormone-independent prostate cancer [9].

Previous studies have evaluated the antitumor activity of ascorbate (vitamin C or VC) and menadione alone (vitamin K_3 or VK_3). Furthermore, the antitumor activity of a VC and VK_3 combination has been evaluated against a series of human carcinomas cell lines, including DU145, which is an androgen-independent prostate cancer cell line. In those studies, the VC and VK_3 combination exhibited higher cytotoxic action than either vitamin alone [10–44]. In the DU145 cell line, the mechanism of the cytotoxic and anticancer action of VC:VK_3 were also studied using electron microscopy, flow cytometry as well as molecular techniques [18,29,35,36]. Subsequently, the in vivo antitumor activity of the VC and VK_3 combination was examined in nude mice [14,15,28,40].

In this report, SEM and TEM have been employed to examine the cytological changes and damage induced by the in vitro exposure of DU145 cells to ascorbate and menadione in order to better understand the vitamin-induced, ultrastructural, cytotoxic changes observed in treating DU145 xenotransplants in nude mice that were observed in another study. Specifically, descriptions of the changes in overall cell morphology and the cell surface are followed by descriptions of the changes in the nucleus and nucleolus, the mitochondria, the lysosomes and other subcellular components and inclusions. While other forms of cell death can occur in vitro in the bladder [19,21,22] and ovarian carcinomas [23–27] as well as in the solid xenotransplants [40,41], the major consequences of this cell damage are tumor cell shrinkage and cell death primarily by a process we named autoschizis [19,21,22,28,32,43].

MATERIALS AND METHODS

The cell line

Human prostate carcinoma (DU145) cells were purchased from the American Type Cuture Collection (ATCC, Rockville, MD). After reception of the frozen cells, they were thawed and centrifuged at 1000 rpm for 10 min. Following removal of the supernatant, DU145 cells were resuspended in 90% Minimum Eagle Medium (MEM, Eagle; Gibco Labs, Grand Island, NY) supplemented with 10% Fetal Bovine Serum (FBS) and 50 μg/mL gentamycin sulfate (Sigma Chem Co, St Louis, MO) and cultured at 37 °C in 5% CO_2. Ascorbate sodium (VC) and menadione bisulfite (VK_3) were purchased from Sigma Chemical Company (St Louis, MO) and were dissolved in phosphate-buffered saline (PBS) to create 8000 μM VC, 500 μM VK_3 and 8000 μM VC/80 μM VK_3 test solutions.

Treatment of cells

Two 12-mm circular glass coverslips or two 100-mesh gold grids were placed in a 35 mm Petri dish. Each dish was seeded with 1.0×10^6 DU145 cells suspended in MEM containing 10% FBS. After 24-h incubation at 37 °C in 5% CO_2, the MEM was removed and cells were washed once with 3 mL of PBS (pH 7.2). Cells were then overlaid with either 6007 μM ascorbate sodium (VC), 77.2 μM menadione bisulfite (VK_3), or VC:VK_3 mixture (312 μM: 3.1 μM) combination. These values correspond to the CD_{50} doses for the vitamins following a 1 h exposure time as determined by a microtetrazolium (MTT) assay [18,29,35,36].

Collection of cells for microscopic examination

MEM-treated cells were used as the Sham-treated control. After 1 h of incubation at 37 °C and 5% CO_2, the supernatant was removed and the cells were rapidly washed twice with 3 mL of PBS. Glass coverslips and grids covered by DU145 cells were transferred to another Petri dish with two 100-mesh gold grids to be examined with SEM. The DU145 cells that adhered to Petri dishes following all treatments were harvested by soaking them free from the monolayer with No-Zyme (JRH Bioscience, Lenexa, KS), centrifuged at 1000 rpm for 10 min and then prepared for transmision electron microscopy (TEM).

Scanning electron microscopy

After each of the treatments, the DU145 cells were fixed at room temperature (18 °C) for 1 h by immersion in 3.2% glutaraldehyde-buffered solution (0.1 M Na cacodylate, pH 7.32). After two rapid rinses in sucrose cacodylate buffer (SC), the samples were post-fixed for 30 min at room temperature in 1% aqueous osmium tetroxide:ruthenium tetroxide (1:1). Following fixation, the samplers were washed four times in SC buffer and dehydrated through graded ethanol. Critical-point drying and sputter-coating were performed as described in [18]. Gold-coated samples were observed with a Jeol JSM-35C SEM set at 15 kV emission of accelerating voltage.

Transmission electron microscopy

The pelleted cells and the cells on coverslips were washed in SC buffer before they were dehydrated by graded ethanol and embedded in PolyBed epoxy resin (Polysciences, Warrington, PA). Sections of 1 μm in thickness were stained by toluidine blue, and selected areas were ultrathin cut of about 400–550 nm thickness, collected on 75- and 100-mesh hexagonal copper grids (SPI Supplies, West Chester, PA). The sections were then contrasted by uranyl acetate and lead citrate prior to examination in the Jeol 100S transmission electron microscope operated at an accelerating voltage of 80 kV.

RESULTS

Fine structure of Sham or untreated negative control DU145 cells: Figures 1(A–C), 2(A–C), and 3(A–F)

Figure 1 illustrates SEM views of aggregated and overlapping DU145 cells as they appear in culture. These cells are often pleiomorphic, polygonal and nearly confluent with some spherical shapes (due to cell division) with diameters ranging from 12 to 17 μm. In this effect, tumor cells exhibit a squamous aspect and, when stretched on the culture support, can reach diameters up to 25 to 35 μm. Detailed views of their abundant microvilli and interdigitating, corrugated lamellipodia-like extensions of the surface are observed in Figure 1(B) and (C). Even though troughs or crevice-like spaces seem to separate adjacent cells (Figure 1C, and in the A area of Figure 1A), the demarcation of each cell remains unclear and some cell overlap or at least discrete contacts appears to occur.

Figures 2(A–C) and 3(A–F) illustrate the TEM aspects of Sham-treated DU145. Tumor cells can be found in clumps and collected regardless of whether they were cultured on cover slips or harvested and pelleted for TEM. They resemble the aggregated arrangements seen in SEM with intercellular spaces and few to no specialized, intercellular, contacts. While Sham-treated cells are pleiomorphic, they maintain a semblance of a polygonal profile and possess a uniform coating of simple to multifurcate microvilli and/or filopodia which are 0.5 to 2.5 μm in length (Figures 2A, 3B–C and E). While the majority of microvilli have a narrow root and tenuous stem, some of the longest ones possess a wide, irregular-sized base and tenuous extension(s). The complex cell coat with multifurcate pattern often intermingles with the cytoplasmic extensions of adjacent cells (Figure 2B). Rare, specialized contacts are found in cytoplasmic extensions less than 0.5 μm in length (Figure 2C). Finally, the cell membranes do not appear to show any damage due to centrifugation or cell processing for TEM, except for minute foamy whorls that rarely decorates the cell profiles (Figures 2A, 3B and E).

The nuclei of Sham-treated cells appears spherical, is usually deeply indented and resembles those in found in xenotransplanted DU145 tumors in nude mice [40]. The nuclear to cytoplasmic ratio is also high (Figures 2A and 3A). In most cells, the nuclei are euchromatic and contain a nucleolus that is large and branching and is associated with one trough of the invaginated envelope. Each nucleolus is rich in nucleolar organizer centers or NORs which is characteristic of highly active, transcribing cells. It is common to find annulate lamellae in the perikaryal areas (Figure 2D).

The most numerous cytoplasmic organelles are the mitochondria which mingle with smooth and rough endoplasmic reticulum (SER and RER) networks and often appear as slender, branching, elongate to cylindrical structures with a few cristae and pale matrices (Figures 2A, E and 3A, F). It is quite difficult to detect a Golgi apparatus as illustrated in Figure 3(D). The numerous electron dense bodies (d = 0.2–2.5 μm) distributed among other organelles in the perikaryal areas likely represent the lysosomal bodies. Many of the cells contain vacuoles of diverse size (Figure 2A) located near glycogen patches and round, lipid droplets (d = 0.2–1.5 μm). These lipid deposits are found in the outermost regions of the cell cytoplasm and occur either individually or as doublets groups which fuse together (Figures 2A, 3A–C). The vacuoles themselves may be fatty deposits which were extracted during the processing of the samples. In some cases, at higher magnification, one can see fatty storage droplets adjacent to or inside glycogen patches (Figures 2A, 3B–C). Furthermore, in some sections, it is possible to detect keratin filaments near the edge of cells (Figure 3C) or within the lamellipodia (Figure 3E). The glycogen patches are numerous and appear as poorly contrasted areas of the cytosol. Polyribosomes and isolated ribosomal particles are observed throughout the same cytoplasm. It is not uncommon to find annulate lamellae in the perikaryal areas (Figure 2D).

Injuries caused by ascorbate- or VC-treatment in DU145 cells: Figures 1(D–F), 4(A–D), and 11(C)

SEM images illustrate that, in contrast with Sham-treated DU145 cells which are pleiomorphic, ascorbate-treated DU145 cells are more often spherical. VC-treated cells possess cell coats with numerous, long microvilli (some reaching 2.5 μm in length) as well as ruffles or shorter lamellipodia, while Sham-treated cells exhibit by either club-shaped or round, globular cell projections (Figure 1D–F).

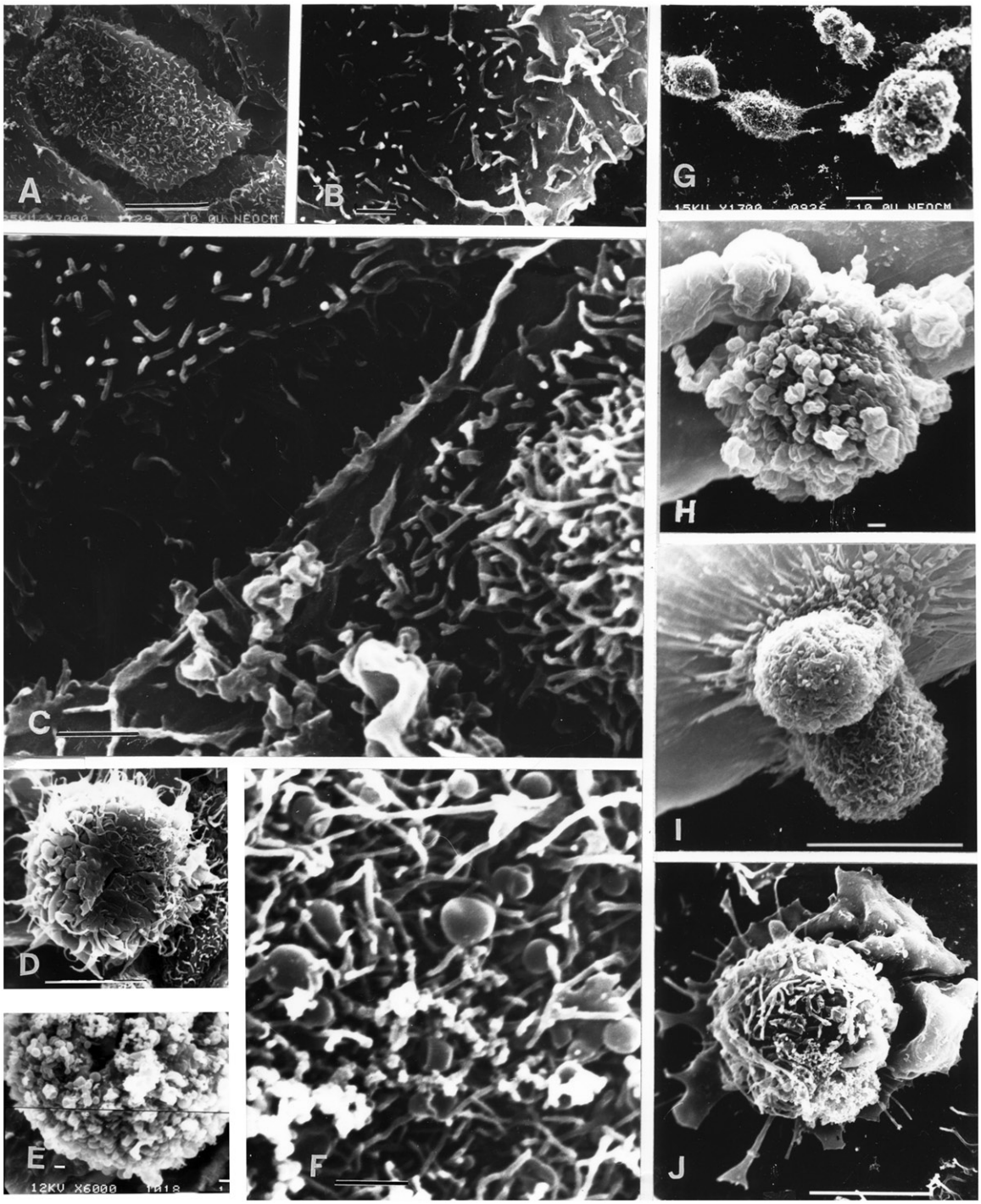

FIGURE 1. A–J: SEM represents selected views of DU145 carcinoma cells following Sham- (A–C), VC (D– F), VK3 (G–H) and VC:VK3 (I–J) treatments. A–C: Sham-treated cells display a pavimentous morphology and are coated by innumerable microvilli and long, narrow lamellipodia along the cell's edges. These surface projections intermingle with each other adjacent cells. The scale in A is 5 μm, while the scales in B–C are 1 μm. D–F: Ascorbate-treated cells exhibit a more spherical morphology and microvilli with pointed edges (in D and F) and lamellipodia with bulbous ends. (E). Cell debris can be found adjacent to cells and coating their surfaces (in F). The scale bar in D is 10 μm and in E–F the bar is 1 μm. G–H: VK3-treated cells are visible as either isolated cells or clumps of cells (G). In H, one can see the heterogeneous cell surfaces of two adjacent cells. One cell displays a smooth surface with large blebs, while the other cell possesses lamellipodia with bulbous, dilated ends and resembles the cells in pane E. The scale bar in G is 10 μm while the scale in H is 1 μm. I–J: Cells obtained following exposure to the VC:VK3 combination. Pane I shows a self-excising cell attached to a golden bar grid. Pane J shows a cell undergoing autoschizis. The cell is self-excising large cytoplasm pieces like petals of a flower, while the main cell covering is made of microvilli and lamellipodia. The scale bars in I and J are 10 μm.

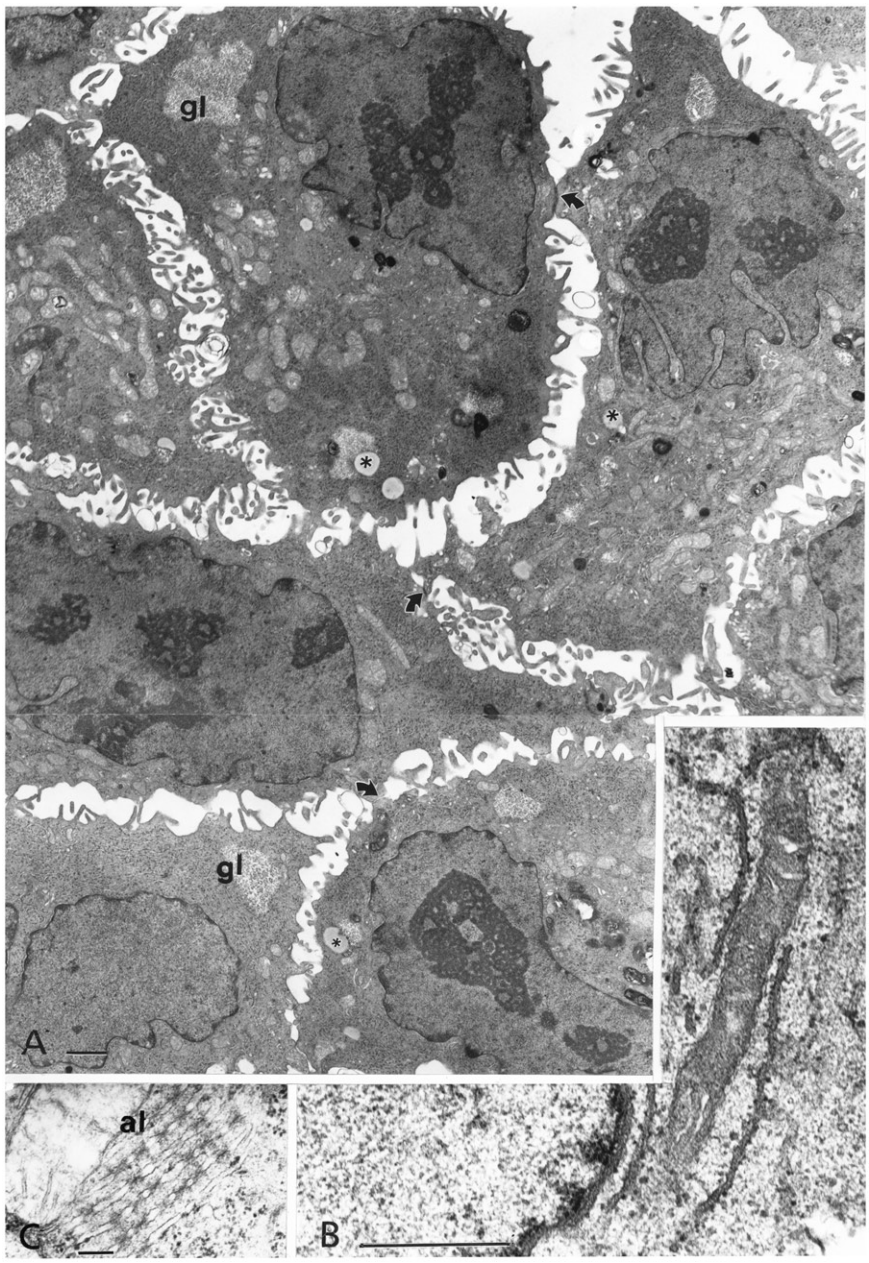

FIGURE 2. A–C: TEM aspects of Sham-treated DU145 carcinoma cells. A: This low magnification micrograph demonstrates the pleiomorphism and the high nuclear: cytoplasm ratio of these cells. The loose cells' aggregation shows poorly differentiated cell junctions (curved arrows). Most contacts between cells are through intricate intermingling of the cell surface extensions. Notice the deeply indented nuclei and their branching nucleoli, the mitochondria population, glycogen (gl) and fatty storage droplets (*). B–C: Both panes shows perikaryal areas containing dispersed rough ER, ribonucleoproteins and glycogen and illustrate in B: A well-contrasted, elongated and quasi-orthodox mitochondrion; in C: A typical annulate lamellae (al) adjacent to a large, low-contrasted mitochondrion. Notice that the perinuclear space is filled with some fine, contrasted material. All scale bars equal 1 μm.

While the TEM views suggest that ascorbate-treated cells are similar in size to Sham-treated, cell remnants found in the intercellular spaces are indicative of self-excisions. However, there were not a sufficient number of cells available to verify this phenomenon. As was the case in the SEM views, VC-treated cells appeared more spherical than the polygonal profiles seen in the Sham-treated cells (Figure 4A–C). The cell coats of VC-treated cells were highly variable with some cells exhibiting abundant microvilli (Figure 4A–C), while others were devoid of microvilli and showed only folded, smooth surfaces (Figure 4B). In many cases, the cell surfaces demonstrated smaller filopodia than the sham-treated ones. The cells with smooth surfaces displayed only minute distortions with the coating extensions less than 50 nm in length.

Following ascorbate treatment, the nuclear profiles did not show the deep invaginations that were seen in Sham DU145 nuclei. Instead, the invaginations in

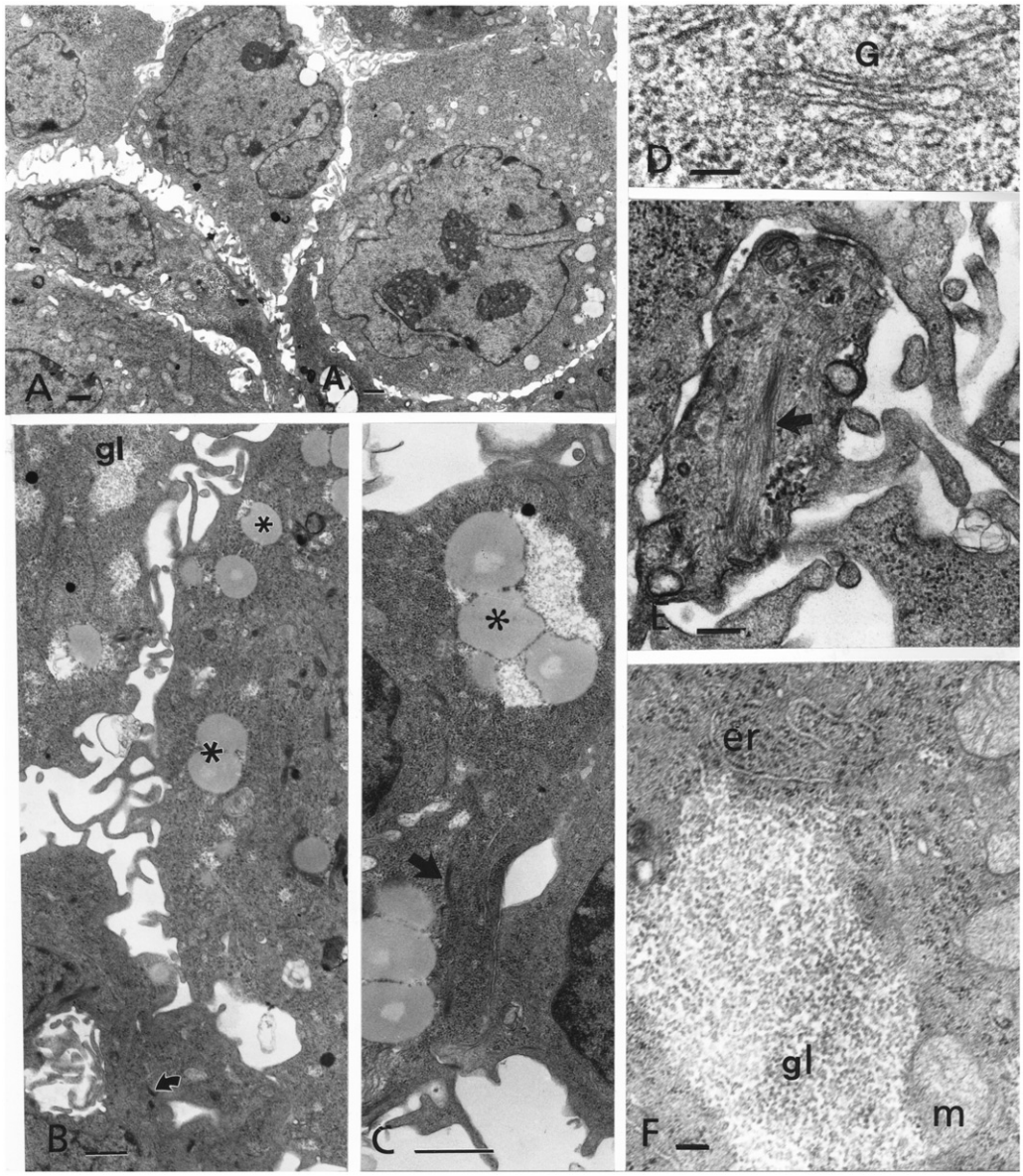

FIGURE 3. A–F: TEM views of organelles and storage products of sham-treated cells. A: This low magnification view of the tumor cells illustrates their scant cytoplasm, indented nuclei, prominent nucleoli; glycogen patches and fat droplets that appear a small vacuoles throughout the cytoplasm. B–C: Higher magnification views of fat (*) and glycogen deposits which are solitary or associated with and within one another. In C arrow marks a thick bundle of cytokeratin filaments. D: An example of a small Golgi apparatus which is usually poorly defined. E: This pane represents a thick cell extension with its cytokeratin cytoskeleton (arrow). F: This pane shows a cytoplasmic glycogen patch surrounded by polysomes, smooth ER and mitochondria. All the scales in A–C are 1 μm and the scales in D to F equal 200 nm.

the round to oblong nuclear profiles were larger with broader openings to the cytoplasm. Nucleoli can be seen among a thin, marbled, euchromatic nucleoplasm. Sometimes, the nucleoli become associated with the nuclear membrane near the invaginations as if they were thick heterochromatin (Figure 4C). In general, the nucleoli were more compact than in the Sham cells. However, because of their branching morphology coupled with the random direction of sectioning, their appearance may be highly variable and range from strongly contrasted, dense compact masses with innumerable, narrow interstices (Figure 4A) to as compact masses which lack interstices, nucleolar organizer regions (NORs) and dense fibrillar regions (Figure 4B).

Among the other organelles, the pale-contrasted mitochondria stand out against the fine, ribosome-rich, granulated and contrasted cytosol. Contrarily to the Sham-treated cells, the mitochondria showed almost wash-out cristae. Furthermore, majority of the mitochondria exhibit whorl-like inner membrane defects and contain electron dense deposits in their matrices (Figure 4A–B). At higher magnification, fields of ribosomes were seen in the cytoplasm. In Figure 4(D), degranulated RER networks extends into SER structures. Similarly, lysosomal bodies can be

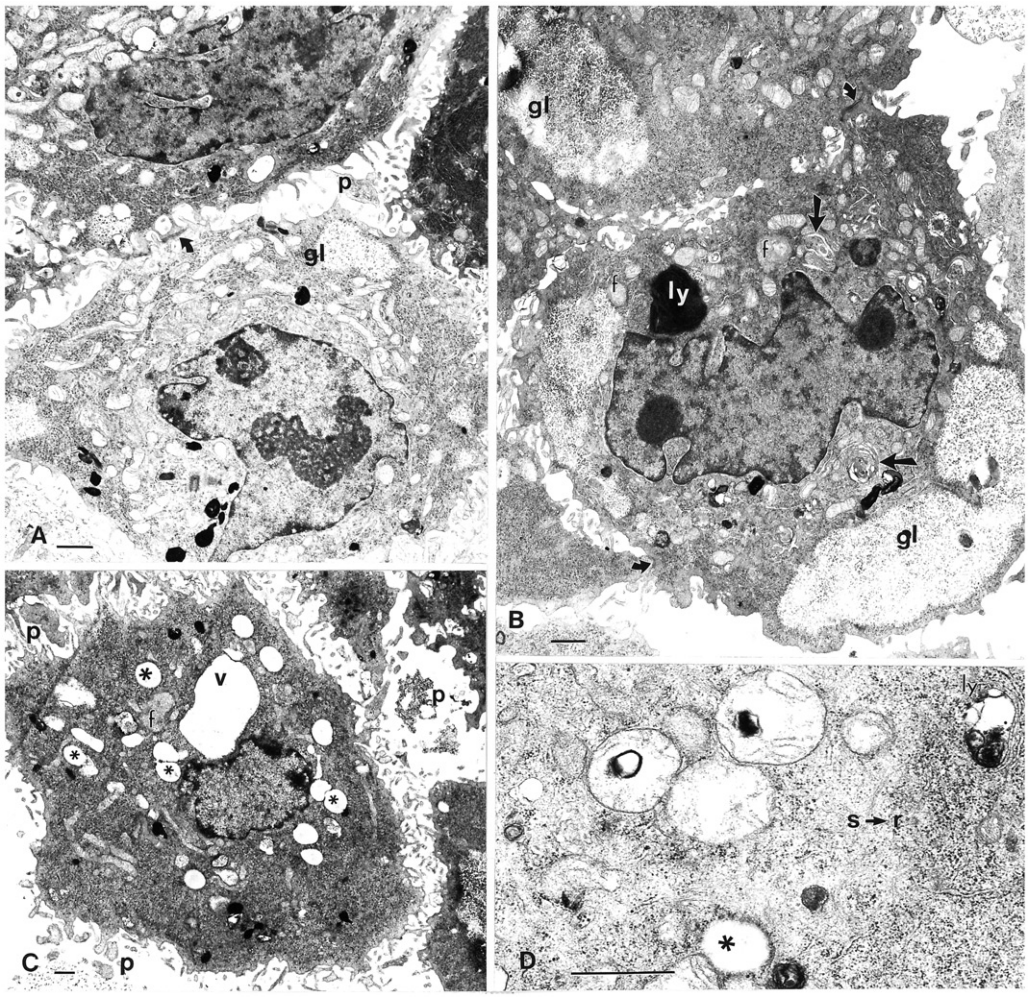

FIGURE 4. A–D: TEM views of VC-treated DU145 carcinoma cells. A–C: These panes contain examples of tumor cells with variably contrasted cytoplasms containing small, spherical lipid droplets (*) and other variable sized, elongate or irregularly-shaped vacuoles. Pale-contrasted mitochondria with visible intramatrical bodies and other cytoplasm fibrillar deposits (f) can also be seen. Immense, swollen glycogen patches can be seen (gl) to be surrounded by ER cisterns. Lysosomal bodies (ly) of variable size, often, some heterogeneous, contrasted bodies with some that may be under formation (straight arrows in B). Cell contacts are marked by small curved arrows (e.g. in A and B). Pieces of cells (p) are scattered in the intercellular spaces. D: Mitochondria (m) with matrices containing distorted cristae and highly electron contrasted, membranous whorls and contrasted deposits are visible. The area labelled s→r illustrates a transition zone from smooth ER to RER. An innumerable amount of polyribosomes and ribonucleoprotein particles are distributed unevenly in the cytoplasmic transition zone. All scale bars equal 1 μm.

recognized as heavily contrasted, heterogeneous bodies of diverse size (0.1–3.5 μm) with the largest ones being found in the perikaryal areas. It is also not uncommon to detect membranous whorls and organelles organizing into autophagosome bodies, even among the endomembranes of the RER-SER (e.g. Figure 4B and D). In the same areas, secretory-like vesicles containing a fine, fibrillar material can also be seen (Figure 4B–C). Most cells still contain a few, clear fatty deposits, but their content is often partly or entirely extracted during the processing of the samples (Figure 4A–D). These deposits can appear as twin droplets (star label in Figure 4C) or can be associated with a lysosomal body (Figure 4D). In addition to those fatty droplets, a number of cells display empty, membrane-lined vacuoles. The origin of these vacuoles is unknown, but they may emanate from the fusion of fatty deposits into enormous lakes as suggested in the cells illustrated in Figure 4(C) or from the outer nuclear envelope as empty and dilated, damaged RER. Finally, there are enormous glycogen patches in most cells. These unevenly contrasted islands can contain small, highly contrasted, irregularly-shaped membranous whorls among the glycogen aggregates and can be interpreted as small autophagosomes or SER membranous defects ''sinking'' into those energetic reserves as those now contain useless debranching enzymes (Figure 4B). Some of the larger glycogen patches can appear fuzzy and poorly contrasted which is suggestive that some of their contents may have been depleted or are being depleted as a food source by the treated cells. In fact, in Figure 11(C) a typical example of glycogen patch, partly digested after treatment can be shown.

Injuries caused by menadione bisulfite- or VK3-treatment in DU145 cells: Figures 1(G–H), 5(A–F), 6(A–D), and 7(A–F)

SEM of VK_3-treated cells reveals a high degree of pleiomorphism. While this treatment usually induces loss of cell- to- cell contacts and leads to separation of the cells (Figure 1G), clumps of heterogeneous aggregates can also be seen (Figure 1H). The nature of these aggregates is difficult to ascertain using SEM and they may represent cell blebbing, cell fragments or cells of a smaller size.

As noted in Figure 1(G), the treated cells are extremely heterogeneous with respect to both cell size and shape with cell shape ranging from flattened, to spherical, oblong and even sausage shaped. This wide variability suggests treatment-induced alterations in the cellular cytoskeleton. Cells can appear as enormous because of cytoplasmic flattening which leaves large areas of the cytoplasm without organelles

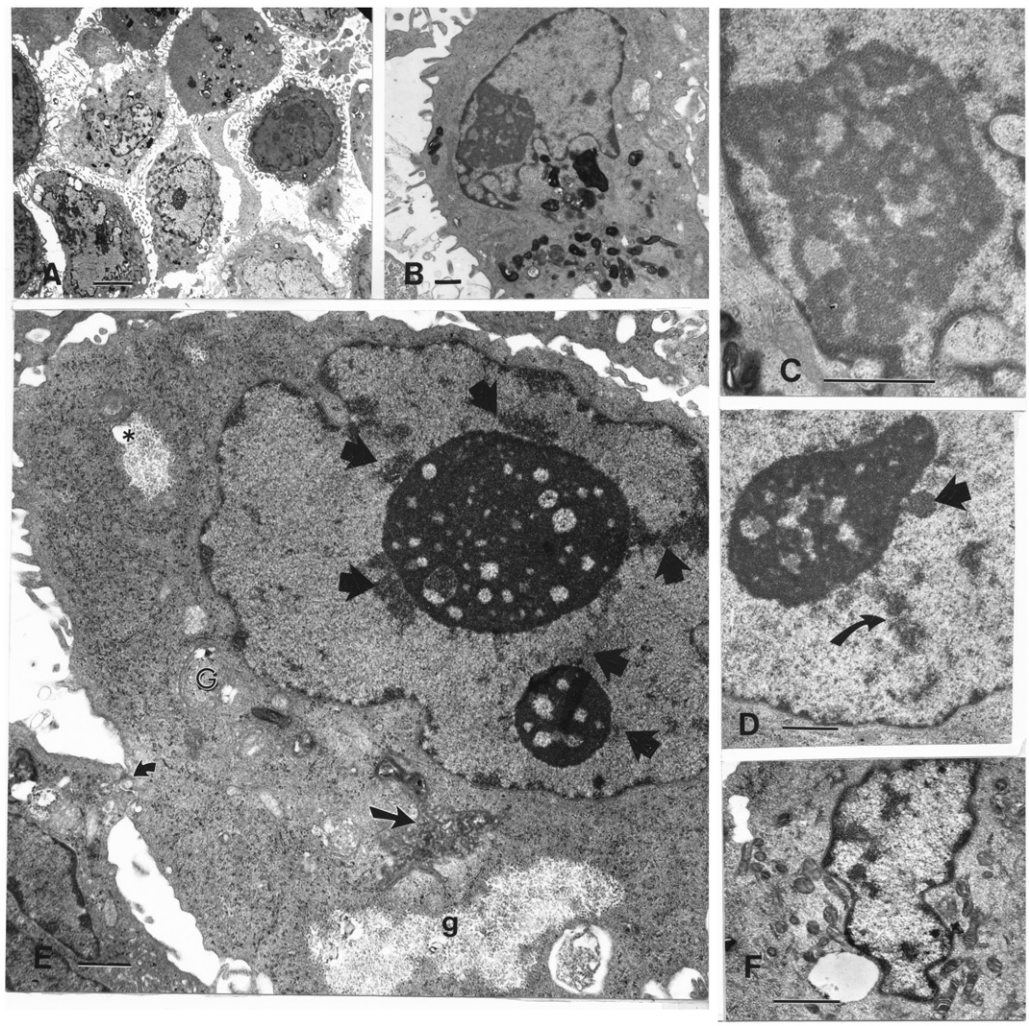

FIGURE 5. A–F: TEM views of VK3-treated DU carcinoma cells with early nuclear changes. A: This pane illustrates the diversity of cell shapes and sizes as well cells content following VK3-treatment. Note that nuclei are more round than lobed and they appear to mirror the cell shapes. Scale equals 5 μm. B–F: These micrographs show nucleolar damage and their elevated electron dense contrast. Pane B shows the apparent nuclear euchromaticity accompanied by a cytoplasm filled with highly contrasted organelles (see Figure 7). These organelles are associated with concavities of the nuclear membrane. Scale is 1 μm. Pane C is an enlarged view of B showing the contrasted, marbled nucleolus which is mainly composed of its ribonucleoproteins. The chromatin associated with nucleolus is heavily contrasted and also decorates the inner nuclear membrane as long dense patches. It seldom is seen as patches in the adjacent nucleoplasm. The scale is 1 μm. Pane D depicts another condensed nucleolus with a sieve-like aspect, a round bulge of chromatin (thick arrow) and irregularly-shaped, electron-dense patches punctate chromatin aggregates (curved arrows). Pane E is a higher magnification image illustrating nucleolar condensation with small and large sieve-like nucleolar interstices. Note that chromatin is extruding in radiating fashion from the nucleolus (thick arrows). A cell contact is seen (curved arrow) as well as a glycogen (gl) patch, a lysosome and highly distorted and contrasted mitochondria (straight arrow). The scale is 1 μm. Pane F shows a cell where the nucleus contains some fibrillar patches; those replace the spheroid remnant of the nucleolus. Vacuoles and condensed mitochondria are also visible. The scale is 1 μm.

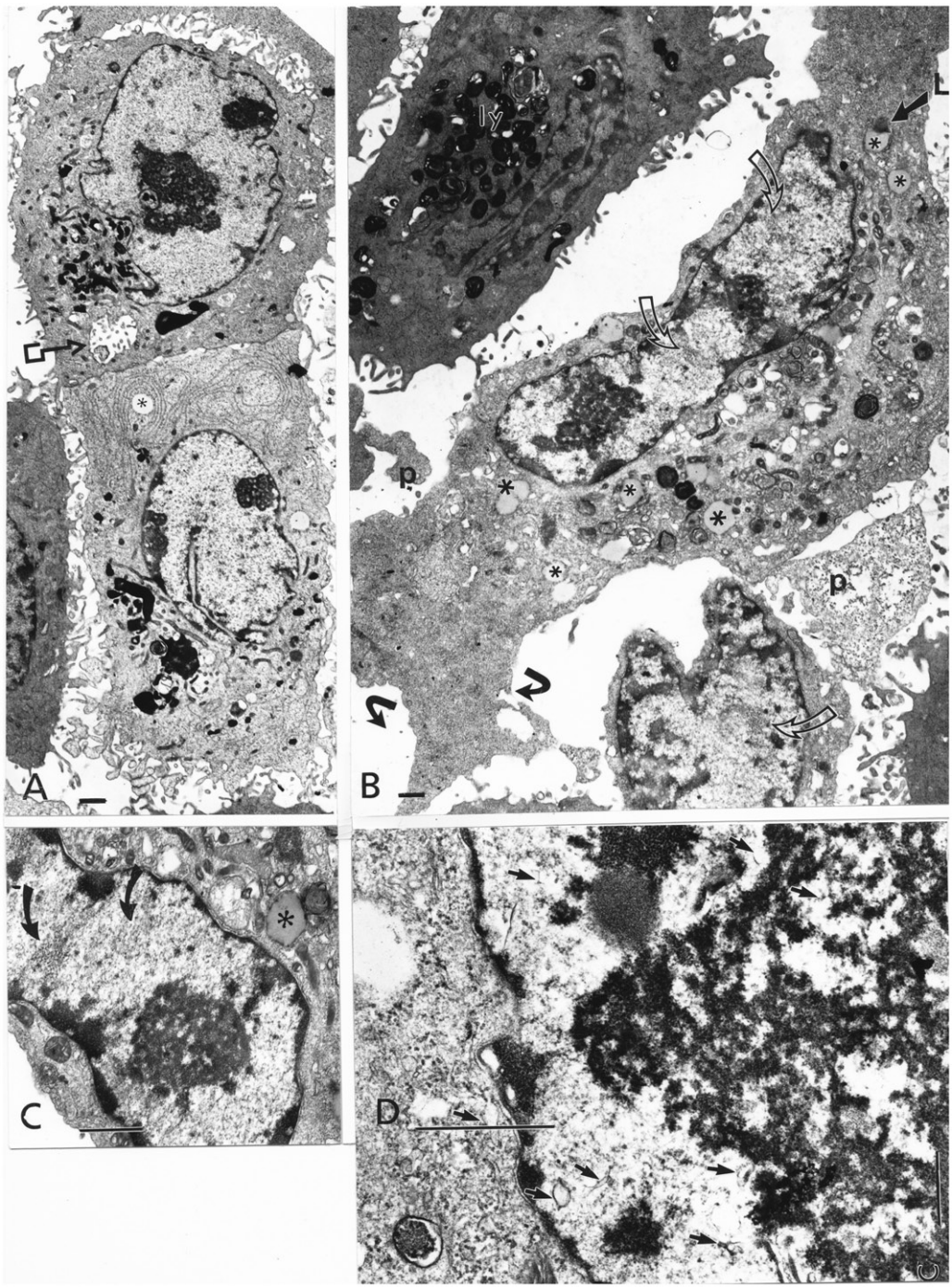

FIGURE 6. A–D: TEM views of VK3-treated DU145 carcinoma cells show cell pleiomorphism with elongated and small size cells containing round, elongated or lobed nuclei containing highly contrasted nucleolar masses. In pane A, the perikaryal areas of the two cells doublet display an intracellular lumen (squared end arrow), numerous, small and oblong lysosomes with all other highly contrasted, damaged organelles aggregated near the nucleus. Most of the remaining cytoplasm is filled by a crowded mixture of elongate RER, ribonucleoproteins, fat droplets and glycogen particles. The nucleoli are condensed and adjacent to the nuclear envelope. Their sieve-like appearance is due to the segregation of their components (see Figure 5 and text). B: Enlarged view of some cells that reveals a variable shape and contrast. All nuclei reveal moth-eaten nucleoli and patches of interchromatin granules [IGs] (open curved arrows). C: An example of condensed but altered reticulated-like nucleolus. IGs are noted (curved arrows). The chromatin associated with the nucleolus displays an enhanced contrast after VK3 treatment and appeared to have left the nucleolus to form nucleolonemal strands in the perinucleolar areas. D: Enlarged area of C that demonstrates the heavily contrasted nucleolar reticulum with interstitial, fuzzy patches as well as several fragments of intranucleoplasmic membranous strands (small arrows) which mingle in the nucleolar interstices. The scales in A–C equal 1 μm and the scale in D equals 0.5 μm.

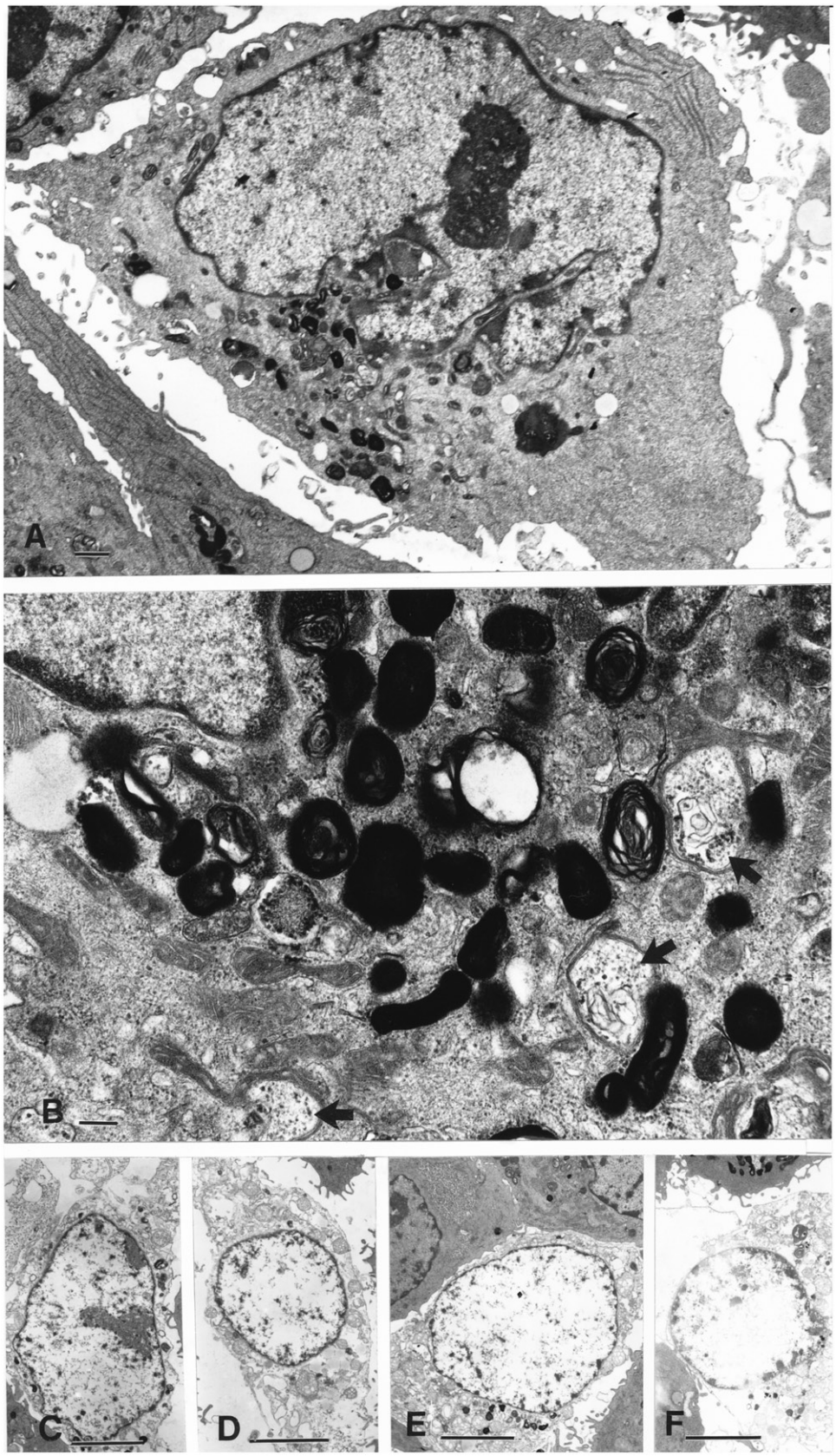

FIGURE 7. A–F: TEM views of VK3-treated DU145 carcinoma cells that depict highly contrasted organelles and cells undergoing autoschizic cell death. A: An example of large cell with highly contrasted nucleolus with segregating (heterochromatin) components with less contrasted interstices. The chromatin appears as clumps outside the nucleolus and along the inner nuclear membrane. IGs are uniformly, spread granules in the nucleoplasm. In the indented nuclear cove, which is usually managed by the centrosome,

continued

other than ribosomes (Figure 5A). The fact that abundant cellular debris can be found in the extracellular spaces is consistent with self-excision events. Heterogeneity is also apparent of the cell surfaces, because some cells or portions of their surfaces have microvilli which can reach 1.5–2.5 μm in height, while others do not display any extensions (Figure 1G–H).

VK_3-treated cell size decreased precipitously to less than 10 μm in diameter through a series of cytoplasmic excisions (Figure 7C–F). In addition, these cells underwent the typical nuclear and cytoplasmic changes characteristic of autoschizic cell death which ultimately led to chromatolysis. During this process, the nucleolar components continued to degrade along with the chromatin while a few altered organelles are maintained in the perikaryal cytoplasm. Once the chromatolysis is completed, the cytoplasm swells and is degraded and the nuclear envelope is disrupted and its contents are dispersed in the cytoplasm.

Electron micrographs obtained from many areas of the 1-μm thick sections reveal many cell fragments in the extracellular spaces as those described with SEM (Figure 5A–C). A large percentage of these VK_3-treated cells also exhibit alterations in multiple organelles that are characteristic of cytotoxicity and are indicative of autoschizic cell death (Figure 6C–F). For example, while the nuclei are often indented (Figure 5A–C), the cells with most cytotoxic alterations exhibit spherical nuclear profiles with wavy membranes and depressions in the shape of shallow grooves. This pattern is typical of proplasia where the outline of the nuclear is ''thrown into waves or undulations'' in an effort reach a maximal area for its volume [54]. As a result of this treatment, the nucleoplasm appeared euchromatic, but it was not because the cells were synthetically active because the nucleoli were compact and often without any heterochromatin associated with them.

The micrographs in both Figures 5 and 6 illustrate most of the nuclear changes induced by VK_3 treatment. One of the initial changes entails the loss of the contents of the nucleolar interstitial spaces and the disappearance of the NORs. In Figure 5(B–C), the heterochromatin lines the inner nuclear membrane as a continuous rim except at the nuclear pores. The nucleolar-associated chromatin appears to be withdrawing from the body of the nucleolus and coalesces with the chromatin along the inner nuclear membrane (Figures 5C–E, 6B–C). As a result of these heterochromatin (DNA) extrusions, the densely-contrasted nucleoli appear to be perforated by the round, pale staining interstices (Figures 5B–D, 6A–C, 7A). The vacuoles adjacent to the nuclear envelope (Figure 5F) following VK_3-treatment cells are more typically observed following VC-treatment (Figure 4A).

Following the extrusion of the heterochromatin, nucleolar compaction can be preserved for a while but ultimately is lost and the nucleoli are seen as fibrillar bundles (Figure 5F) or with a thick, reticulated morphology (Figures 6A–D, 7C–F). These nucleolar changes are accompanied by the segregation the fibrillar and granular components with the fibrillar portion appearing as a loose, darkly contrasted network. This contrast may be due in part to greater osmium binding to the calcium which was attracted as a counter ion to the menadione (Figure 6B–D). Simultaneously, arrays of interchromatin granules (IGs) appeared as punctuate dots ($d < 20$ nm) clustered between heterochromatin clumps in the nucleoplasm (Figure 6B–C curved arrows), and similar structures noted in Figure 7(A). IGs were also detected following VC and VC:VK_3 treatments.

In other organelles, alterations were noted in the mitochondria (Figures 6A–D, 7A–B) and the lysosomes exhibited altered morphology (Figures 6B, 7A–B). The elongated mitochondria were profoundly distorted with distorted, narrowed matrices containing tiny granulations. The pleiomorphic mitochondrial matrices are caused by distorted inter membranous space and elongated cristae (Figure 7B) and somewhat condensed and contrasted matrical spaces. The lysosomes often appeared either as onion bodies with membranous contents or with flocculent and granular content often detected as autophagosomes or in process of becoming or making autophagosomes (Figure 7A–B). In addition, both organelles became highly contrasted following VK_3 treatment. This enhanced osmiophilia also noted in the previous paragraph is believed to be a function of a VK_3-induced increase in Ca^{2+} in the mitochondria internum and the consequent accumulation of osmate

Continued

numerous diversely contrasted organelles are noted including: lysosomes, of heterogeneous size and content as well as fat deposits and vacuolated bodies whose contents may have been extracted during processing for TEM. Other poorly differentiated cytoplasmic areas contain some RER and free ribonucleoproteins. Cell pieces surround the cell. The scale equals 1 μm. B: An enlarged area of the perikaryal cytoplasm contains many electron contrasted organelles. The most contrasted organelles are lysosomal bodies which appear as tightly- coiled round, onion bodies whose contents cannot be resolved. These lysosomes admixed with mitochondria that are elongated, bent or warped and whose matrices are contrasted with a heterogeneous, speckled, filamentous, and grainy content (e.g. arrows). The scale equals 200 nm. C–F: A series of micrographs depicting the end-stage of autoschizic cell death. These panes show self-excised cells with nuclei, a rim of cytoplasm and altered organelles. The most notable observation was their pale nuclei, with degraded chromatin. After the nucleolar remnants disappeared, the nuclei swelled and final cell demise occurred in F after the nuclear envelope ruptured. The scale is 5 μm.

salts [45]. Typically, these highly-contrasted organelles became congregated in a jumbled fashion near the concave surface of an eccentric nucleus (Figure 6A–B) via a disrupted microtubule tracts lead under the direction of the centrosome. Likewise, the lysosomes display almost the same osmiophilia as the mitochondria with an intense contrast often obstructing the view of their contents (Figures 5A–B, 6A–C and 7A–B).

Other organelles can be observed throughout the finely granular cytoplasm. Abundant rough and SER were evident (Figures 5A, 7A), while Golgi apparatus (Figure 5E) and intracellular lumina (Figure 6A) are of small size and challenging to be detected and only visible in some cell sections. Many deposits of glycogen can appear as large patches with widths of 5–8 μm (Figure 5E). Fatty deposits in the form of droplets were detected as well preserved (Figure 6A–C) or poorly preserved (Figure 7A) due to extraction during the preparation of the cells.

Injuries caused by ascorbate and menadione bisulfite- or VC:VK3-treatment in DU145 cells: Figures 1(I–J), 8(A–E), 9(A–G), 10(A–E), 11(A–B), and 12(A–D)

SEM views reveal that VC and VK_3 treatment results in spherical cells ($d < 15$ μm) which are smaller than sham treated cells (Figure 1I–J). These spherical cell bodies are coated with extension exhibiting widely diverse shapes. Large pieces of the cell which are being excised surround the cell body and resemble the petals of a flower (Figure 1J). Other cellular debris can be observed around the cells (Figure 1I).

As was the case with the SEM micrographs, TEM micrographs demonstrate a reduction in cell size due to self-excisions following exposure to the vitamin combination. Likewise, there is an increased prevalence of cytoplasmic vacuoles. In addition, a smaller number of cells were present following exposure to the vitamin combination than in either single vitamin treatment because of increased cytotoxicity and subsequent loss of cell adherence to the substrate (Figures 8C–D, 9E, 10A). Most cells that remained contained a large nucleus with altered chromatin and an altered nucleolus (Figure 8A–D).

Figure 8 demonstrates nuclei undergoing chromatolysis, while nucleoli fragment and appear minute contrasted patches alongside the heterochromatin patches on the inner nuclear membrane (Figure 8A). Other injuries include swollen mitochondria as well as a rim of cytoplasm containing fatty deposits that appear as droplets alongside injured nuclei. In some cells (as noted in Figure 8A, C–D), large lysosomes similar to those described after VK_3 treatment are visible (e.g. Figures 7A–B, 8A and E). In Figure 7(E) isolated fibrillar deposits appear in some cells and resemble aggresomes. Finally, most remaining large tumor cells reveal glycogen patches with a moth-eaten aspect (Figure 8C).

Figures 9 and 10 illustrate nuclear and nucleolar alterations following a combined vitamin treatment. In the selected cells, the nucleoplasms showed fine granulation resulting from heterochromatin dilution and disaggregation. In addition, some cells found in the 1-μm thick sections are binucleated which confirms blockage in cell cycle described in [29]. Figure 9(A–D) shows the segregated components of the nucleolus with a progressive condensation of the granular component producing a huge mass with a few sieve-like perforations caused by the interstices or from where the chromatin was extracted (Figure 9A–B) to a ring-shape (Figure 9C) and/or an odd topology as a football-shaped mass (Figure 9D). Further nucleolus damage can be illustrated in Figure 9F–I where its nadir produces a dismantling and fragmentation of the granular masses. In Figure 9G–I, an advanced, chromatin degradation (chromatolysis) is shown because only small heterochromatin patches are persisting, attached to the inner nuclear membrane, while fine granules seeded the nucleoplasm and appeared in the same size as the IGs found earlier. Maybe these IGs are actually the products of further nucleolar fragmentation (Figures 8A–E, 9A–I and 10A–D). The significant and progressive decrease in the contrast of the heterochromatin suggests a DNase-mediated degradation of its DNA content verified in other tumor cell lines. Figure 9(E), in particular, illustrates the end of karyorrhexis for a group of three DU145 cells with thick packets of heterochromatin outside of the nucleoli as well as along the peripheral nucleoplasm and the inner nuclear membrane. From Figures 9F–I and 10A–D, the nucleoplasm contains smaller nucleolar remnants and IGs as well as diminished contrast due to progressive DNA lysis or chromatolysis, until cell demise by autoschizis. The nuclear envelope remains apparently intact until the perikaryal cytoplasm is self-excised or bursts due to osmotic swelling of the remnants (Figures 10C–E, 11A–B), which then is often accompanied by rupture of the nuclear envelope (Figure 10E) after or while the nuclear envelope seemed to have lost integrity. Previous to oncotic bursting the nucleus, the outer nuclear membrane pores and membrane showed series of blisters (Figure 11B) while the cytoplasm has vacuolations and remnants of organelles (profoundly altered mitochondria and autophagosomes of diverse size) can be noted. Fatty deposits and glycogen can be found throughout the final stages of cell demise to death and are ultimately degraded and expelled in the intercellular spaces along with other remaining cytoplasmic components (Figure 10A–D).

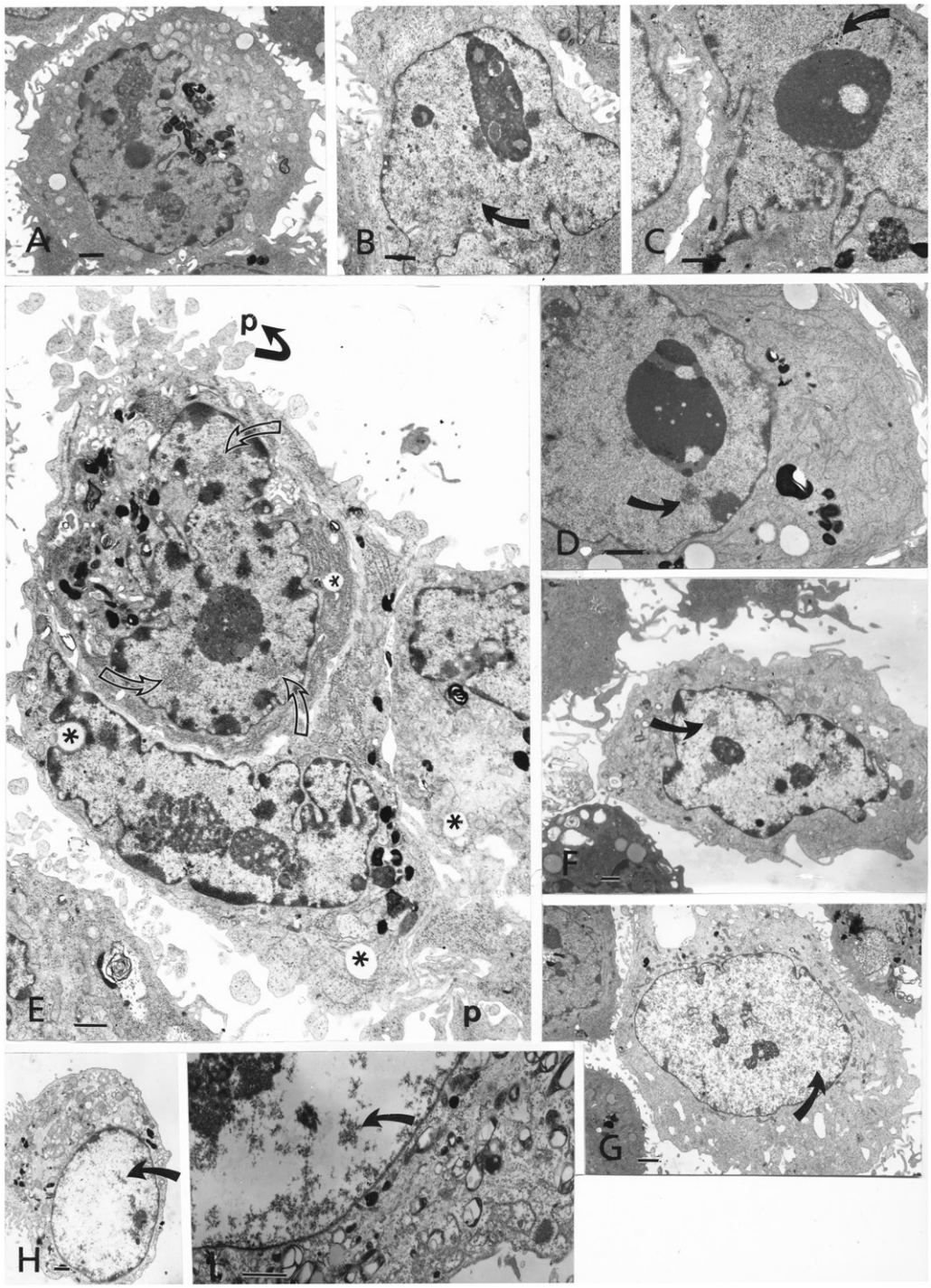

FIGURE 8. A–I: TEM views of VC:VK3-treated DU145 carcinoma cells. A–D: These panes represent selected examples of cells after VC:VK3-treatment. Usually these cells were small and approximately spherical in shape. The displayed nuclei with progressive degradation of the chromatin whose nucleoplasms become sequentially less contrasted, while their nucleoli become sequentially more and more condensed and contrasted due to their masses of mainly ribonucleoproteins (granular components) which can remain tightly aggregated as doughnut, in C or as football shaped, in D). Initially, the altered nucleoli maintained some fine fibrillar and interstitial components (in A–D). (E–I): Further segregation of the nucleoli, resulted in the secession of the chromatin as packets into the nucleoplasm which appeared as bursts of material at the nucleolar edges. E: An example of cells remaining from VC: VK3-treatment showed cells with high nuclear: cytoplasm volume ratio, nucleoli condensed into large or elongated, reticulated, nucleolonemal masses of ribonucleoproteins and chromatin packets dispersed in the peripheral nucleoplasm. Most organelles were swollen or vacuolated and possessed a narrow rim of remaining cytoplasm. G: In this pane, a more advanced chromatolysis is illustrated, with small packets of heterochromatin along the inner nuclear membrane. H: This cell demonstrates further chromatolysis with nucleus becoming rounder than in sham-treated cells; I: This pane gives a detailed view of IGs and swollen organelles (small mitochondria and lysosomes). All IGs are indicated throughout by curved arrows. All scale bars are 1 μm.

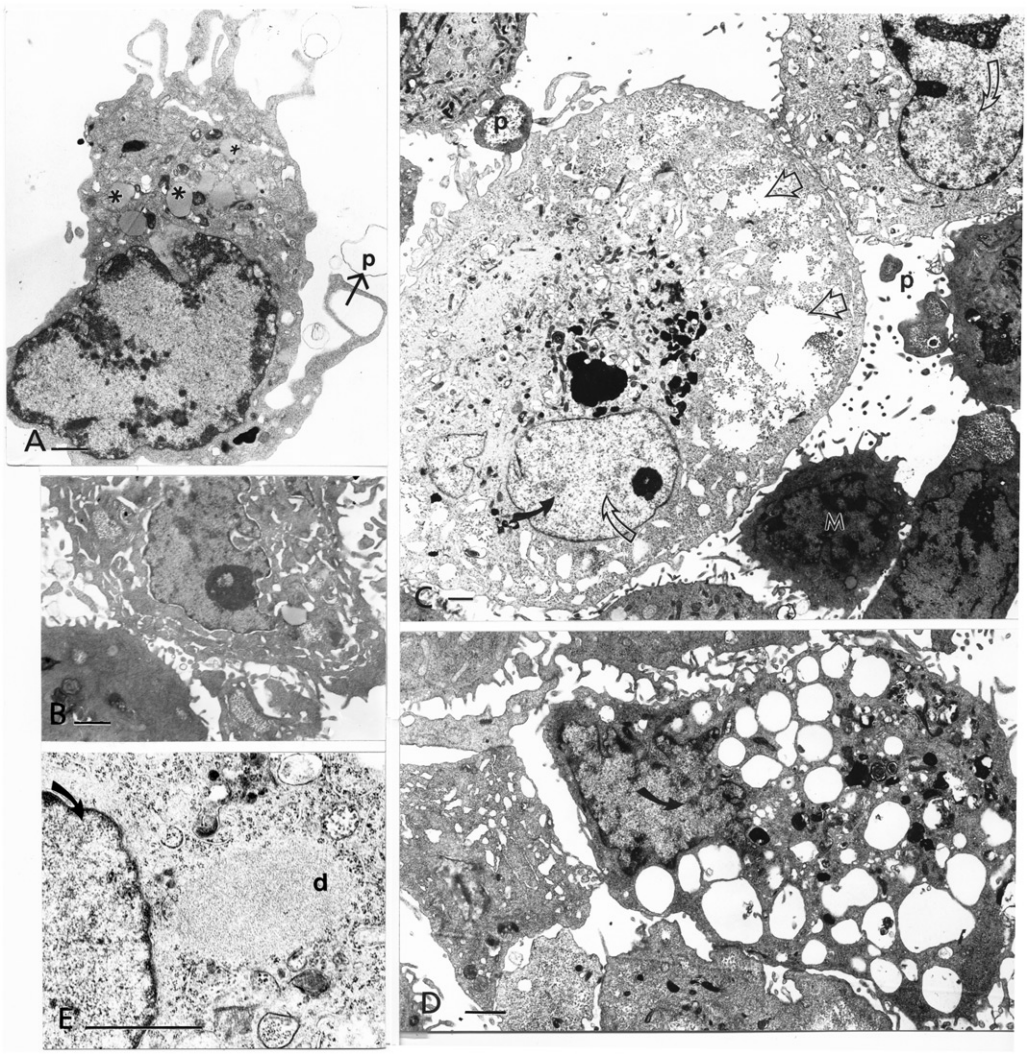

FIGURE 9. A–E: TEM views of VC:VK3-treated DU145 carcinoma cells and autoschizis. This panel further summarizes cell pleiomorphism and damage leading to cell death by autoschizis (see also Figure 6A–D). Specifically, cell size decreases, nuclear alterations appear and the cell self-excising pieces of cytoplasm and membrane (p). A: Example of a treated cell containing an enormous nucleus and a uniformly, poorly contrasted nucleoplasm containing condensed heterochromatin along the inner nuclear membrane. Nucleolar fragments can be seen within the peripheral zones of the nucleoplasm. Self-excisions through vacuoles and trailing appendages can be seen. B: A cell with nucleolar condensation and numerous vacuoles, as well as cell debris. C: Pale DU145 cells are surrounded by small, diminished (M) cells produced by self-excisions. Debris consists of pieces (p) of cells still containing glycogen are in the intercellular spaces. Darkly contrasted lysosomes, vacuoles and moth-eaten glycogen patches are noted (clear arrows). Nuclei are altered and show highly compacted, broken nucleoli and interchromatin granules (IGs; curved dark and pale arrows). D: Example of a damaged cell with an increased number of vacuoles amidst lysosomal bodies and a nucleus where no nucleolus can be found. E: This is part of a vacuolated cell containing an ellipsoid-shaped deposit (d) made of fine fibrillar material. Its nucleus shows IGs (curved arrow) and is surrounded by altered ER and lysosomes. The scale bars in A–E equal 1 μm.

DISCUSSION

Ultrastructural aspects of Sham-treated DU145 carcinoma

Sham-treated DU145 cells are pleiomorphic and appear round to flat with their margins overlapping when they are confluent [46]. DU145 cells are poorly differentiated and typically display a typical coat of innumerable, irregular size microvilli [47] with a diversity of odd shapes [48] as previously noted [18,29,40,41]. They have a large, active nucleus and scant cytoplasm. Therefore, these cells have a high nuclear to cytoplasmic ratio that is consistent with most malignancies and the nuclear membrane exhibits ''unpredictable'' and unexplainable irregularities [49,50] as well as cytoplasmic indentations which often gives the nucleus a coffee bean shape [51]. The nuclear profile typically possesses a deep or shallow indentation that can be called ''pocket, bleb, canal, tubular invagination'' or ''infolding'' [52]. These invaginations are often a diagnostic of poorly differentiated cell [53], increase the surface area to volume ratio of the nucleus and can facilitate the sustenance

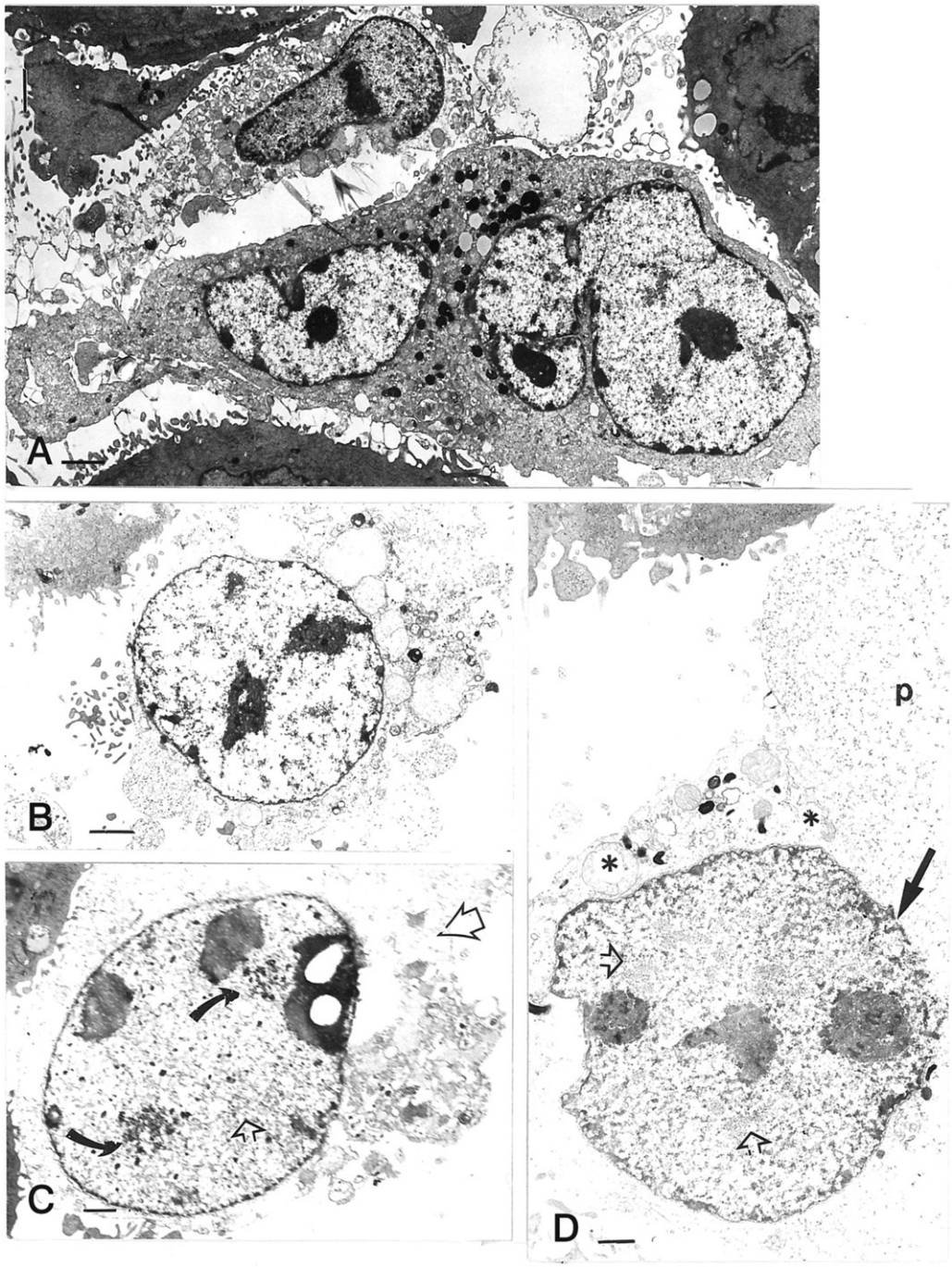

FIGURE 10. A–D: TEM views of VC:VK3-treated DU145 carcinoma cells and autoschizis. A: A binucleated DU145 cell is visualized amongst injured cells and pieces (p) and remnants of dying cells. The large cell displayed chromatin dissolution as well as compaction of the nucleolus and possessed well-contrasted lysosomes. B–D: These electron micrographs are examples of DU145 cells undergoing cell demise by autoschizis. The micrographs set shows that autoschizic cells kept their nuclei intact during the dissolution of their chromatin and formation of their nucleolar remnants and IGs (curved arrows and short open arrows) until the ultimate stage of cell demise (in D). In pane B a small, bubbly rim of cytoplasm with swollen organelles was seen. C: This pane showed further cytoplasmic shedding pieces until blebs of the last pieces of cytoplasm (large open arrow) were gone. In this example, it was possible that some nuclear pores of the nuclear envelope served as puncture sites as the nucleus bloated. D: This pane showed the ultimate stage of extrusion with nuclear lysis and nucleoplasm (p) bursting along with the cytoplasmic remnants, using the punctured nuclear envelope (open dark arrow in D). All the scale bars equal to 1 μm.

of the nucleoplasm reticulum [54] as well as enhance cytoplasmic-nuclear and facilitate cytoplasmic-nucleolar exchanges because the nucleoli are often localized near the termini of these nuclear envelope invaginations. These changes in nuclear shape are often influenced by cytoskeletal changes that have also been associated with alterations in specific transduction activities [55] and with tumor

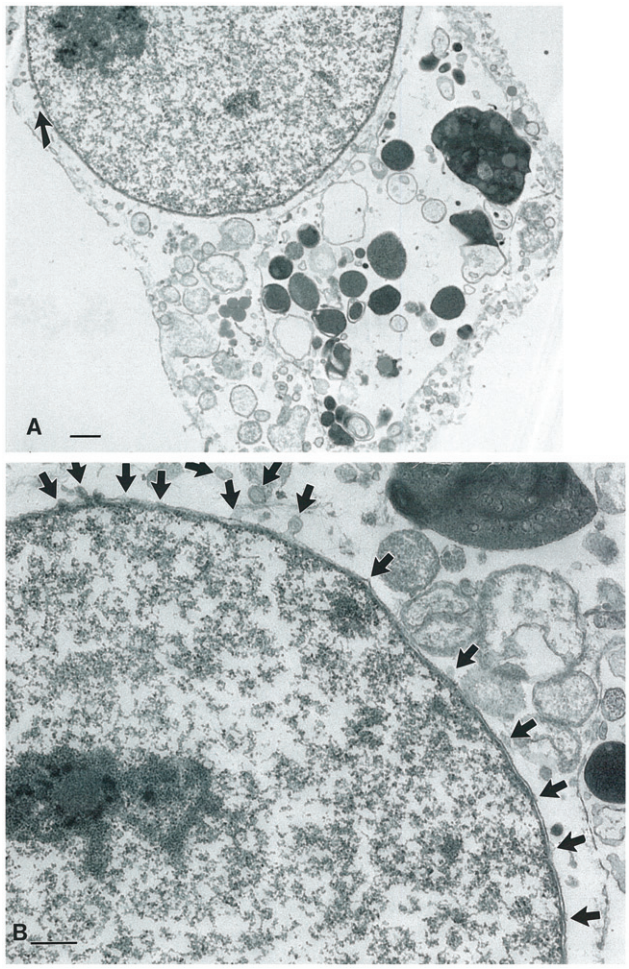

FIGURE 11. A–B: Example of a VC:VK3-treated DU145 carcinoma cell undergoing final demise by autoschizis; its lower (in B) and upper region (in B). The nuclear envelope is still lining a swollen nucleus with bursting nuclear pore structures (especially the outer membrane component, ribosome-free; as indicated by small arrows) is surrounded by altered remnants of organelles (mitochondria and electron densely-contrasted lysosomal bodies) haphazardly distributed in vacuolated cytoplasmic remnants. Scales in A is 500 nm, in B is 200 nm.

suppressor gene activity [56]. Finally, these cytoplasmic invaginations are often rich in F-actin [23,53,56] and can be pathways along which transcripts move into the cytoplasm [57]. The nucleoli of those nuclei often contain multiple NORs [58–61] which is characteristic of extremely active cells [82] and poorly differentiated tumor cells [61–63].

While the cytoplasm of these cells exhibit a paucity of organelles, such as the SER and the Golgi apparatus and exhibit no apparent secretory products [41], they do possess an abundance of RER. Intracytoplasmic lumina and annulate lamellae are also typical of these cells [41,42] as the latter appear to be involved in synthesizing membranes of the nuclear envelope and RER [63]. Lysosomes are seen as homogeneous or heterogeneous phagosomes. The cytosol is filled by innumerable ribonucleoproteins and/or ribosomes,

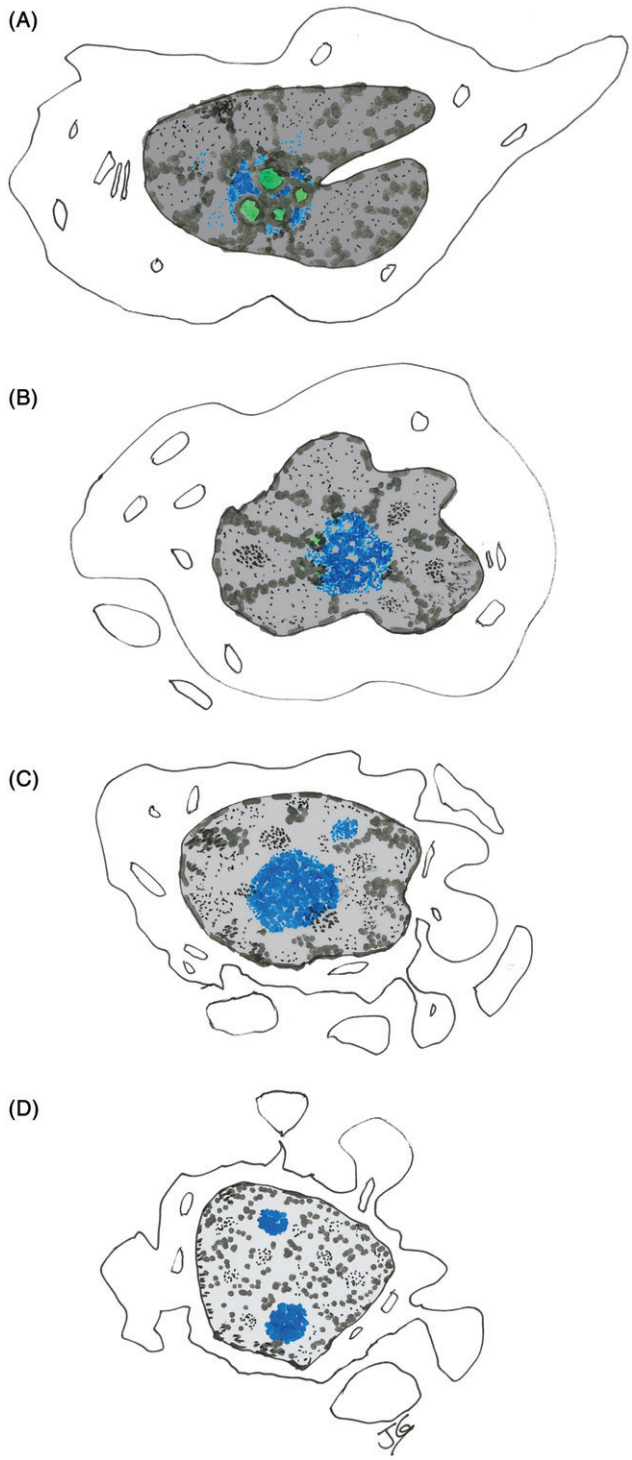

FIGURE 12. A–D: Diagrammatic representation of DU145 carcinoma cells with the major nuclear alterations leading to autoschizic cell death. During nuclear changes, the nuclear envelope remains apparently intact until the cell demise. Cytoplasmic self-excisions reduce the cell size until a rim of cytoplasm remained, but nuclear size was maintained. Cytotoxic changes of the cytoskeleton are not represented. Intrinsic nuclear structure damage noted during injurious DNase, RNase and ROS damaging activities are: (i) a progressive decreased euchromatic DNA content as found in previous reports. This is marked by a fading intensity of grey from A to D; (ii) black tracings mark the heterochromatin

continued

a feature which is also found during liver carcinogenesis [64] and may reflect the loss or inactivation of RNases during cell transformation or a typical characteristic of tumor cells [15] As in many other tumor cells, fat and glycogen deposits accumulate in DU145 cells.

Cytotoxic alterations of DU145 cells caused by ascorbate- or VC-treatment

During the last 45 years, the ability of ascorbate or VC to treat or prevent cancer has been tested because of its antioxidant properties. However, recent evidence suggests the cytotoxic activities of VC may be related to its pro-oxidant properties [65]. Regardless of the mechanism of action, VC exerts selective toxicity in vitro toward several tumor cell lines and those results were noted in vitro [22,26–28,35,36,66] and against tumor cells in vivo [17–22,32,35,36,67]. VC is also a chemosensitizing agent [12,13] and a radiosensitizing agent [14,68]. Various mechanisms have been proposed to explain the antitumor properties of ascorbate but no evidence has been presented to adequately explain the preferential attack on the primary tumor cells or their metastases, as opposed to normal cells. The explanations have been reviewed in several of our recent publications [15,19–29,32,33,36,39,66].

The earliest ultrastructural studies from Lupulescu [67] showed neoplastic cells exposed to VC exhibit membrane and cytoskeletal disruptions, mitochondrial changes, and a small reduction in nuclear and nucleolar size and some autophagocytotic activity. Likewise, the results of the current study show VC treatment induces a small reduction in nuclear and nucleolar volume compared to other carcinoma cell lines [18–28,30–33,66]. The presence of small pieces of cellular debris in the intercellular spaces in many micrographs supports these contentions and agrees with previous flow cytometry data [29]. Already Szent-Györgyi [69] suggested that the cycling of VC between ascorbate and dehydroascorbate would result in a concomitant oxidation of glutathione and other intracellular macromolecules rich in thiols including depletion of thiol residues of those of the nuclear cytoskeleton [70,71] as well as initiate numerous membrane lipid peroxidations [72]. Through unrepaired membrane defects cascades of intracellular signals would eventually lead toward tumor cell death [73]. Lipid peroxidation of the superficial protoplasm can account for: (i) the increased fluidity of the cell membrane then causing elongation of the filopodia without microspikes and other superficial alterations [19,21,22,26,27]; (ii) the destruction of Ca^{2+} homeostasis [74–76]. These changes in turn could lead to potentiation of nuclease and endoprotease activities [76], increased thiol oxidations, and poisoning of the mitochondria which in turn would lead to significant ATP depletion, and lower the safe level of cell energy charge [77] that ultimately would favor cell damage through irreversible repair and fatal cytotoxicity.

In the majority of cells, the nucleoli acquire a compact aspect visualized as either spherical, electron dense bodies in contact with the nuclear envelope or as thick, electron-dense patches in contact with a rim of chromatin in a diminutive nucleus. Those latter nucleolar aspects are consistent with a late G_2 block of the cell cycle where the dense and fine fibrillar components are excluded from a mass of synthesized ribonucleoproteins following damage of the intrinsic nucleoskeletal components caused by peroxidation and DNase action [78]. Most nuclei showed retroplasia as shrinking activity following VC exposure may have modifications in the nuclear infrastructures. One has noted that IGs can be seen in the nucleoplasm of most cells with IGs' concentration consistently relating with the amount of nuclear and cell damage. Mitochondrial membrane alterations after fixation are not as easily detected, but small whorls-like changes have been observed [26,27,66,79].

There are a number of potential candidates that could account for the ultrastructural damage following VC exposure. Taper and his collaborators [10,15,17] have shown that DNase II (E.C. 3.1.22.1) is one such candidate. In the cytoplasm DNase II is bound in a 1:1 complex with a repressor protein. Acidification of the cell reactivates DNase II by releasing it from its repressor. Recent studies suggest that DNase II is combined with an anti-apoptotic, serine protease inhibitor, leukocyte-elastase inhibitor (LEI) and that acidification allows separation of LEI from DNase II which creates an active lysosomal-DNase II [80]. The acidification of the cytoplasm

Continued
features as parts of its nucleolar dense fibrillar component (also named chromatin-associated with the nucleolus) that is being excised and appears to be leaving the nucleolus for the perinucleolar, nucleoplasm (iii) the disappearance of fine fibrillar region of the nucleolus (in green, from A to B) and the interstices forming at first a nucleolonema as an entangled network of ribonucleoproteins (in blue). The ribonucleoproteins as granular component of the nucleolus then form a more or less large mass that can fragment or can disappear entirely (not represented). Concomitantly, the heterochromatin is then seen with a decreased condensation along the inner membrane of the nuclear envelope. It initially appears as a thick, contrasting layer that thins along with the nuclease digestion and progressively loses contrast and becomes innumerable dots or particulates through chromatolysis. IGs are represented by small clusters of dots between the strands of heterochromatin. Accompanied by other cell injuries, internal osmotic forces created by the accumulated small molecular species force the nuclear envelope to break at some weakened places, i.e. dilating a few nuclear pores, then bursting and dispersing the remainder cell contents as a corpse. Based on this report and accumulated data reported in text (e.g. Gilloteaux et al. [19,25,26,27,66] and Jamison et al. [29,32,43]).

required to reactivate DNase II suggests permeabilization of the lysosomal membrane with the release lytic enzymes including cathepsins [81]. Lysosomal permeabilization was verified morphologically after similar treatment of RT4 bladder carcinoma cell line [27].

Cytotoxic alterations of DU145 caused by menadione bisulfite or VK_3-treatment

VK_3 is a synthetic derivative of VK_1 whose antitumor activities have been studied for at least 50 years. It exhibits a broad spectrum of cytotoxic activity in vitro against many human tumor cell lines and those were noted in our previous reports [15,26,27,35,36,66] including other studies on urological tumors [35,36,82,83]. VC is equally potent against multiple drug-resistant and drug-sensitive cells, as well as against human tumor explants derived from patients that are refractory to other types of chemotherapy. While at least a portion of its antitumor activity may be due to the ability of VK_3 to induce cell cycle arrest or delay at both the G_1/S and G_2/M phases of the cell cycle [29,35,36], the majority of its antitumor properties are attributed to its pro-oxidant properties and poison tumor nucleoside metabolism [84].

VK_3 is indeed a well characterized pro-oxidant or oxidant that can stimulate growth, trigger apoptosis or cause necrosis depending on its dose and time of exposure [85]. For example, 5 μM VK_3 stimulates DNA synthesis and promotes mitogenesis, while 10μM VK_3 exerts anti proliferative effects, 20 μM VK_3 can induce apoptosis and 100 μM VK_3 induces necrosis [86]. Menadione-induced defects are dose and time dependent and can include many intracellular defects reviewed in previous studies [22,23,25–37,41,66]: (i) a significant depletion of reduced glutathione (ii) a reduction of the cell ATP pools; (iii) oxidation of sulfhydryl groups in cytoskeletal proteins and associated macromolecules [87]; (iv) reactivation of DNase I and the subsequent degradation of tumor cell DNA [10–13,15,35,36,88] and (v) a deregulation of cellular Ca^{2+} sequestration can impede the phosphorylation of ERK and/or of other regulating factors of the cell cycle [89,90]. Like VC, the cycling of VK_3 results in the production of reactive oxygen species (ROS) which can damage the antioxidant defense by drawing down cell thiols, interfere with protein folding, alter signal transduction [91], and promote degradation of histones and keratin [92].

Tumor cells are sensitive to this oxidative stress because they typically have lower levels of the enzymes necessary to detoxify ROS than non-transformed cells [93]. While the coordinate attack of ROS may induce membrane damage in the exoplasmic regions in the form leakiness and blebs and prepare the cell for cytolysis [94], VK_3 predominately affects the cytoskeleton, as noted above [92], and especially nuclear actin [95–97]. The superficial actin network is richest and deemed to affect the cell surface morphologic pattern and locomotion much faster than the one of the deeper cytoplasm that influences endo- and exocytoses [97] and is the cytoskeleton first affected by VK_3, hence all intra- and extracellular motility [98]. The cytoskeletal alterations not only included regulatory proteins, but also intrinsic, superficial ones (i.e. spectrin [99], filamins [100]) which led to the changes in cell morphology (i.e. drastic reduction in cell size and pleiomorphic shapes with lamellar extensions) and caused the cells to accumulate the organelles in one same area [18,21–23,25–28,42,101] and as shown in this report.

VK_3 may also affect nuclear and its nucleolar structure. While actin is part of the nucleoplasm and is involved in transcriptional activity [71], it also interacts with tubulin associated with the nucleolus [56]. Because DNase I is bound to G-actin in a 1:1 complex which represses it and it can separate from the complex to make F-actin [102,103], one can speculate that derepressed DNase I could degrade DNA [104,105] and disturb the NORs integrity [106] and other structures of the nucleolus. The vacuous interstices in the nucleolar masses following VK_3 treatment demonstrated that the chromatin (DNA) was absent or degraded. Most cells show a compacted nucleolus with the sieve-like aspects that appeared to be remnants of fine fibrillar centers without the dense fibrillar component (or chromatin) that was excised by DNase. These observations are consistent with the scheme offered by Hernandez-Verdun [78]. These changes affect the overall nuclear architecture and integrity leading to the production of IGs, as noted by Kerr and collaborators in apoptosis [107] and confirmed by Smetana (personal communication in [27]).

Other membrane defects caused by ROS production on lipids moieties can lead to osmotic defects, resulting in dilation of the RER, mitochondrial swelling, enlargement of the Golgi apparatus and lysosomal enlargement and other anomalies. Those anomalies triggered some autophagocytotic activity [27] and could also lead to injuries that liberate ceramide, whose action also could be involved cell death process [108].

Mitochondrial dysmorphology was often present following VK_3 treatment. These organelles appear to have been stretched or squeezed and to have extended in an "effort" to make contact with or become part of the autophagosomes of the damaged cells. The continuity between the outer mitochondrial membrane and the endoplasmic reticulum [109] could certainly facilitate ionic and enzymatic, events leading to autodegradative activities. Injuries to the

mitochondrial envelope by ROS could likely upset Ca^{2+} homeostasis [110] and eventually trigger cytochrome c release to the cytoplasm and induction of apoptosis [111] or other cell deaths, including autoschizis [38,39]. However, it appeared that the majority of VK_3-induced cell death was autoschizis [18–29,35,36,39,43]. Defects of some caspases but not others, creating different internal events that ultimately induce a different cell death than apoptosis [110]. Menadione-induced cytotoxicity on the mitochondria resulted in some swelling and the formation of osmiophilic deposits throughout those organelles. The deposits could be caused by peroxidation of the mitochondrial membranes, with subsequent loss of membrane potential and excessive, unregulated uptake of Ca^{2+}. The peroxidized lipids of the membranes and cysteine groups of the inner thiol content were oxidized allow the inner content to acquire spotty and peculiar osmiophilic deposits caused by calcium ions exchange with osmium salts to become osmate salts similar to that observed in ZIO staining [45]. It is also true for protoplasmic elements where proteins and/or glycoproteins were associated through these bounds [104]. These organelles accumulated as autophagosome bodies in the perikaryal zones as they also interact with the endoplasmic membrane defects as shown in a recent series of degradative events as suggested in starvation [111].

VK_3 treatment promoted increased lysosomal activity through membrane peroxidation. Whorls formation was observed around damaged organelles similar to what Melgar and collaborators [112] noted in mitochondria of the cardiovascular system. They are results of repetitive autophagic events related to lipid peroxidations induced membrane damage [113] as well as others described in the previous paragraph (mitochondria and ER). Those huge, osmiophilic bodies confirm the ongoing autophagocytotic activity. A similar, but slow process, contributes in normal cell aging to an accumulation after long periods of the same autophagosomes as aging or lipofuscin bodies. Their origin are likely mitochondrial and other organelles and their accumulated location likely confirms damage to the microtubular network damage whose centrosome in the nuclear cove is unable to organize and allow lysosomal bodies to reach distal regions of the cytoplasm to be expelled from the injured cells [18,19,22,23,25–28,114].

Cytotoxic alterations of DU145 cells treated by a combination of VC:VK_3

When VC and VK_3 were combined in a ratio of 100:1, the vitamin combination exhibited tumor-specific antitumor activity against human breast, oral epidermoid and endometrial tumor cell lines at doses that were 10–50 times lower than when either vitamin were administered alone [12–14,17,39,115]. Likewise, when the VC:VK_3 combination was administered to a series of 13 human uro-gynecologic tumor cell lines, the vitamin combination exhibited synergistic antitumor or cytotoxic activity at concentrations which were 4- to 61-fold lower than for the individual vitamins [29,30,32,33,35,36,115,116]. Additional studies, using a transplantable murine liver tumor model, showed that the VC:VK_3 combination was an effective chemosensitizer and radiosensitizer [11–16]. These previous studies and those conducted with human tumors in nude mice indicated that the VC:VK_3 combination induced little systemic or major organ pathology [11–16,31,43].

VC:VK_3 combination exerts its antitumor and antimetastatic activities through a wide array of mechanisms described in the aforementioned paragraphs including: blockage of the cell cycle, reactivation of DNases and RNases [15], modulation of signal transduction as well as the redox state of the cell, inhibition of glycolysis and induction of autoschizic cell death [19] or, apoptosis, in the case of leukemia cells [117].

The cytotoxic mechanisms involve controlling tumor cell energetics and biochemistry through coordinate modulation of cellular phosphorylation and/or redox potential. This is possible for two reasons. First, many tumor cells have reduced levels of catalase, superoxide dismutase and/or glutathione peroxidase and as well as glutathione and other ROS detoxifying enzymes. Therefore these cells have difficulty in detoxifying hydrogen peroxide and other ROS which then accumulate, alter cellular processes and induce cellular damage or cell death [43]. Second, because of derangements in mitochondrial ultrastructure and energetics, tumor cells rely primarily on glycolytic metabolism known as the 'Warburg effect' [118,119].

Tumor cells that are not killed by the combination VC:VK_3 (or Apatone) treatment usually exhibit cell cycle arrest. This arrest may be a function of a number of factors including: deficient cell metabolism, defective signal transduction and ultrastructural changes in the nucleolus. Flow cytometry indicates that DU145 cells are blocked at both the G_0-G_1/S interface and in G_2-M [29,33,43]. A significant decrease in cellular DNA content was also observed in an ovarian tumor cell line following VC:VK_3 or Apatone treatment [23–26]. This cleaved DNA may represent the remnants of cellular DNA following the activation of DNase I and DNase II during autoschizis [15,25–28,35,36,43]. This ongoing chromatolysis was demonstrated by light microscope technique (Feulgen stain), by ultrastructure and was also proven by gel electrophoretic data in other tumor cell lines [25–28,43].

The altered nucleolar structure observed following VC:VK_3 (or Apatone) treatment may be a function

of the reactivation of DNases and RNases. The chromatin is seen to leave the nucleolar body until only the ribonucleoprotein mass remains. Once the chromatin is retracted from the nucleolus its DNA was fragmented by the reactivation of DNase I (VK_3) and DNase II (VC) [15,18,25–29,35,36]. The remaining mass of ribonucleoproteins (the granular component of the nucleolus) appears doughnut to football-shaped resembles changes seen following treatment with other anticancer drugs [61,119–124]. The chromatin is progressively lysed by DNases and perhaps lysosomal enzymes [34,81]. To support this contention lysosomal damage was also illustrated in [27,28]. It is again shown in this report that the treated cells' nucleoplasm becomes less and less osmiophilic or contrasted through progressive DNA degradation. A similar extrusion of chromatin and nucleolar changes was reported in fibroblasts following RNase treatment [15,125,126]. Likewise, RNase can also remove subcomponents of the ribonucleoproteinic, granular components [106,127,128] which ultimately remain following chromatin extrusion. Finally, the relocation of fibrillarin in the nucleoplasm appears to be a marker of these nucleolar remodelling during autoschizis [34].

The data collected by electron microscopy suggests a fewer number of cells survived Apatone treatment than survived VC or VK_3 treatment. In addition, most of the cell injuries leading to cell death were consistent with autoschizis as seen in other tumor models including: bladder carcinomas T24 [19,21,22,26,33,129] and RT4 [27], ovarian carcinoma MDAH 2774 [23–25,28,116], murine prostate carcinoma TRAMP [66] and discussed in an educational report [28].

Peculiar structures

Several peculiar structures were observed following VC:VK_3 treatment: IGs, intracytoplasmic deposits and autophagic processes; the latter will be discussed in a future report. The IGs are observed as clusters of osmiophilic dots loosely aggregated in the nucleoplasm making a substructure that appears as result of cytotoxic drug treatment and viral infection. They contain no DNA as they resist to DNases' treatments [130] and are not stained by DNA contrasting stains [127,131]. However, because small ribonucleoproteins have been identified in IGs [132], they could be assembly, or modification, and/or storage sites for proteins involved in pre-mRNA processing. These function(s) would explain their nucleoplasm localization adjacent to a nucleolus [133] that has been dismantled during a complex derangement of its cytoskeleton and other associated insults. Since these IGs were also described in the interphasic nucleus [134], one could speculate that their presence was related to the G_1 block of the cell cycle phase [29]. Alternatively IGs could be remnants of the nuclear matrix skeleton [135]. Regardless of their origin, they were also revealed in the nucleoplasm of other autoschizic tumor cells [23,26,27]. The fact that intracytoplasmic deposits were essentially seen in the perikayal zones of the cell following VC:VK_3 (Apatone) treatment suggests they originated from peroxidative effects on sulfhydryl moieties of proteins, especially the cytoskeleton, and are likely to be displays of misfolded protein accumulations [27,136,137]. These resembled similar deposits found in atrial myocytes in cardiomyopathy [138]. Alternatively, these particulate structures may represent F-actin aggregates. Finally, large autophagic processes were seen in these cells as well as in xenotransplants of DU145 cells [40–42]. Some cells containing huge phagosomes could be caused by the capture and degradation of a neighbouring cell during entosis. Alternatively, these vacuoles could occur during signet cell formation [40–41].

Tumor cell death by autoschizis

The term autoschizis was coined by Gilloteaux to describe the novel type of cell induced by VC:VK3 treatment of tumor cells and the term was first published in 1998 [19] and further details were also published by our research groups in a series of publications [15,19–28,32–34,41,43]. Autoschizis was created from the Greek root "autos" (as in αὐτός "self") and "schizis" or "schisis" (as in "σχίσις") meaning "division" or "cut" from "skhizein" (Greek "σχίζειν") as in "to split") that was then spelled "schizis." As a consequence, the term "autoschizis" signifies "self-cutting" or "self-dividing" because the major steps and events historically observed in this mode of cell death were self-excisions found in most injured cells by pro-oxidants or oxidative stress as in our experiments, altered by the combined VC:VK_3 treatment [19,21,22]. Morphologically speaking, cells undergoing autoschizis maintain an apparently intact nuclear envelope and some perikaryal cytoplasm containing often altered organelles removed by autophagy (Figures 10C–D and 11) while reducing its size by self-excising pieces of its peripheral cytoplasm. The excising cell fragments do not contain nuclear fragments or organelles like those seen in apoptotic bodies [107,139–141] complemented by extrusion of nuclear RNA packets [142]. The tumor cell alterations in autoschizis are morphologically different from those described in apoptosis and necrosis alias oncosis [143]. Furthermore, autophagy, as used here, is preserving its historical definition as it is a means by which a living cell eliminates damaged parts in a sort of self-recycling manner [144–146], as a cell preservation processing by which cells attempt

to preserve themselves against odds [113] and should not be confused with type II programmed cell death [147]. A circum-nuclear location of the injured organelles is certainly confirmed in analogous cytotoxic events [26,27,114] and probably by a reorganization of the cytoskeletal network of the cell as noted in most autoschizic, dying cells.

The most prominent changes in organelles found in autoschizic cell death are the degradation of its nucleus content while nuclear envelope is maintained, inclusive of the segregation of its nucleolus components (as shown in this report) verifying previous data [18–28,42,43,66] as well as of its energetic-making organelles and deposits, as shown in this report. At the point of no return, autoschizic cell injuries show DNA degradation that can be verified at it exhibits a spread pattern following electrophoresis [25,26,28,43] instead of the laddering pattern, as shown in apoptosis [148–150], indicating internucleosomal cuts. Finally, in autoschizis, cathepsins and not caspases can be the cell executioners [81].

Autoschizis means ''self-cutting'' does not necessary indicate death but a event in which cell self-cut piece(s) as in apocrine secretion events. In so doing, one can document normal cell rearrangement of their cytoskeleton to favor apocrine self-cuts or other similar types of cuts. In the case of cytotoxic pro-oxidants this mode of cell death can be induced in tumor cells. Similar morphologic alterations with self-excisions can be found in the literature and have been illustrated there as apoptotic cell death or as some type of programmed cell death. Future investigations could consider autoschizis as a mode of cell self-cutting which, under analogous cytotoxic actions, can eventually result into cell death or cell's alterations without death as shown in the following mammalian examples: cardiac development [151], erythrocyte maturation [152,153], functional prostate epithelium [154] and in Clara cell differentiation [155].

In order to summarize and visualize the main aspects of ultrastructural changes described by fine structure in the nuclei and its nucleoli occurring in autoschizis, as observed in this report, a set of sequential drawings is submitted in Figure 12.

ACKNOWLEDGEMENTS

The authors acknowledge support from Summa Health System Foundation, Akron, OH and from the Hess-Roth Kaminski & Maxon Foundation of Erie, PA. Support also originated from IC-Med Tech, San Diego CA and data were part of the 1st International Symposium on 'Innovative Anticancer Drugs and Strategies', held in Newcastle upon Tyne, June 2010 sponsored by St George's University School of Medicine, Grenada – New York, and Summa Research Foundation, Akron OH. The Symposium was held in memory of Henryk S. Taper, MD PhD, deceased in 2009. Steve Getch, Communication Specialists of Summa and John Workman with Kate Adamson, Northumbria University graphics, are recognized for their contributions in the technical assistance to set the electronic imagery to illustrate this report.

DECLARATION OF INTEREST

The authors declare no conflicts of interests. The authors alone are responsible for the content and writing of this article.

REFERENCES

1. Jemal A, Bray F, Center MM, et al. Global cancer statistics. *CA Cancer J Clin* 2011;61: 69–90.
2. Weir HK, Thun MJ, Hankey BF, et al. Annual report to the nation on the status of cancer, 1975–2000, featuring the uses of surveillance data for cancer prevention and control. *J Natl Cancer Inst* 2003;95: 1276–99.
3. Siegel R, Naishadham D, Jemal A. Cancer statistics, 2013. *CA Cancer J Clin* 2013;63: 11–30.
4. Dall'Era MA, Albertsen PC, Bangma C, et al. Active surveillance for prostate cancer: A systematic review of the literature. *Eur Urol* 2012;62: 976–83.
5. Lees K, Durve M, Parker C. Active surveillance in prostate cancer: Patient selection and triggers for intervention. *Curr Opin Urol* 2012;22: 210–15.
6. Amaral TM, Macedo D, Fernandes I, Costa L. Castration-resistant prostate cancer: Mechanisms, targets, and treatment. *Prostate Canc* 2012;doi: 2012:327253.
7. Harris WP, Mostaghel EA, Nelson PS, Montgomery B. Androgen deprivation therapy: Progress in understanding mechanisms of resistance and optimizing androgen depletion. *Nat Clin Pract Urol* 2009;6: 76–85.
8. Paller CJ, Antonarakis ES. Cabazitaxel: A novel secondline treatment for metastatic castration-resistant prostate cancer. *Drug Des Devel Ther* 2011;5: 117–24.
9. Oudard S. Progress in emerging therapies for advanced prostate cancer. *Cancer Treat Rev* 2012;39: 275–89.
10. Taper HS. Evaluation of the validity of the histochemical lead nitrate technique for alkaline and acid deoxyribonuclease. *J Histochem Cytochem* 1979;27: 1483–90.
11. Taper HS. Altered deoxyribonuclease activity in cancer cells and its role in nontoxic adjuvant cancer therapy with mixed vitamins C and K3. *Anticancer Res* 2008;28: 2727–32.
12. Taper HS, de Gerlache J, Lans M, Roberfroid M. Non-toxic potentiation of cancer chemotherapy by combined C and K3 vitamin pretreatment. *Int J Cancer* 1987;40: 575–9.
13. Taper HS, Roberfroid M. Non-toxic sensitization of cancer chemotherapy by combined vitamin and K3 pretreatment in a mouse tumor resistant to oncovin. *Anticancer Res* 1992; 12: 1651–4.
14. Taper HS, Keyeux A, Roberfroid M. Potentiation of radiotherapy by nontoxic pretreatment with combined vitanins C and K3 in mice bearing transplantable tumor. *Anticancer Res* 1996;16: 499–503.
15. Taper HS, Jamison JM, Gilloteaux J, et al. In vivo reactivation of DNases in implanted human prostate tumors after administration of a vitamin C: K3. *J Histochem Cytochem* 2001;49: 109–19.

16. Taper HS, Jamison JM, Gilloteaux J, et al. Inhibition of the development of metastases by dietary vitamin C: Vitamin K3 combination. *Life Sci* 2004;75: 955–67.
17. DeLoecker W, Janssens J, Bonte J, Taper HS. Effects of sodium ascorbate (vitamin C) and 2-methyl-1,4-naphtoquinone (vitamin K3) treatment on human tumor cell growth in vitro: II. Synergism with combined chemotherapy action. *Anticancer Res* 1993;13: 103–6.
18. Gilloteaux J, Jamison JM, Venugopal M, et al. Scanning electron microscopy and transmission electron microscopy aspects of synergistic antitumor activity of vitamin C-vitamin K3 combinations against human prostatic carcinoma cells. *Scanning Mcrosc Intl* 1995;9: 159–73.
19. Gilloteaux J, Jamison JM, Ervin E, et al. Cancer cell necrosis by autoschizis: Synergism of antitumor activity of vitamin C: Vitamin K3 on human bladder carcinoma T24 cells. *Scanning* 1998;20: 564–75.
20. Gilloteaux J, Jamison JM, Arnold D, Summers JL. Scanning electron microscope characteristics of human prostate adenocarcinoma cell line (DU145) transplanted in nude mice. *Scanning* 1999;21: 106–7.
21. Gilloteaux J, Jamison JM, Arnold D, Summers Jl. Autoschzis: Another cell death for cancer cells induced by oxidative stress. *Ital J Anat Embryol* 2001;106: 79–92.
22. Gilloteaux J, Jamison JM, Arnold D, et al. Ultrastructural aspects of autoschizis: A new cancer cell death induced by the synergistic action of ascorbate:menadione on human bladder carcinoma cells. *Ultrastruct Pathol* 2001;25: 183–92.
23. Gilloteaux J, Jamison JM, Arnold D, et al. Microscopic aspects of autoschizic cell death in human ovarian carcinoma (2774) cells following vitamin C, Vitamin K3 or vitamin C:K3 treatment. *Microsc Microanal* 2003;9: 311–29.
24. Gilloteaux J, Jamison JM, Arnold D, Summers JL. LM and SEM aspects of autoschizic cell death of ovarian carcinoma cells. *Scanning* 2003;25: 137–49.
25. Gilloteaux J, Jamison JM, Jarjoura D, et al. Autoschizis: A new form of cell death for human ovarian carcinoma cells following ascorbate: Menadione treatment. Nuclear and DNA degradation. *Tissue Cell* 2004;36: 197–209.
26. Gilloteaux J, Jamison JM, Arnold D, et al. Morphology and DNA degeneration during autoschizic cell death in bladder carcinoma T24 cells induced by ascorbate and menadione treatment. *Anat Rec A Discov Mol Cell Evol Biol* 2006;288: 58–83.
27. Gilloteaux J, Jamison JM, Neal DR, et al. Cell damage and death by autoschizis in human bladder (RT4) carcinoma cells resulting from treatment by ascorbate and menadione. *Ultrastruct Pathol* 2010;34: 140–60.
28. Gilloteaux J, Jamison JM, Arnold D, et al. Autoschizis: A new cell death induced found in tumour cells induced by oxidative stress mechanism. In: Mendez-Villas A, Alvarez JD, eds. *Microscopy, science, technology, application and education*. Bajadoz, Spain: Bajadoz, Spain, Formatex Research Center. Microscopy, 2011;1: 211–20.
29. Jamison JM, Gilloteaux J, Venugopal M, et al. Flow cytometric and ultrastructural aspects of the synergistic antitumor activity of vitamin C-vitamin K3 combinations against human prostatic carcinoma cells. *Tissue Cell* 1996; 28: 687–701.
30. Jamison JM, Gilloteaux J, Arnold D, Summers JL. SEM view of synergistic effects of vitamins C:K3 on DU 145 prostatic carcinoma cell line. *Scanning* 1999;21: 107–8.
31. Jamison JM, Gilloteaux J, Taper HS, Summers JL. Evaluation of the in vitro and in vivo antitumor activities of vitamin C and K3 combinations against human prostate cancer. *J Nutr* 2001;131: 158S–60S.
32. Jamison JM, Gilloteaux J, Taper HS, et al. Autoschizis: A novel cell death. *Biochem Pharmacol* 2002;63: 1773–83.
33. Jamison JM, Gilloteaux J, Nassiri MR, et al. Cell cycle arrest and autoschizis in a human bladder carcinoma cell line following vitamin C and vitamin K3 treatment. *Biochem Pharmacol* 2004;67: 337–51.
34. Jamison JM, Gilloteaux J, Perlaky L, et al. Nucleolar changes and fibrillarin, redistribution following Apatone © treatment of human bladder carcinoma cells. *J Histochem Cytochem* 2010;58: 635–51.
35. Venugopal M, Jamison JM, Gilloteaux J, et al. Synergistic antitumor activity of vitamins C and K3 on human urologic tumor cell lines. *Life Sci* 1996;59: 1389–400.
36. Venugopal M, Jamison JM, Gilloteaux J, et al. Synergistic antitumor activity of vitamins C and K 3 against human prostate carcinoma cell lines. *Cell Biol Int* 1996;20: 787–97.
37. Zhang W, Negoro T, Satoh KM, et al. Synergistic cytotoxic action of vitamin C and vitamin K3. *Anaticancer Res* 2001; 21: 3439–44.
38. Calderon PB, Caddrobbi J, Marques C, et al. Potential application of the association of vitamin C and K3 in cancer treatment. *Curr Med Chem* 2002;9: 2269–85.
39. Verrax J, Cadrobbi J, Delvaux M, et al. The association of vitamins C and K3 kills cancer cells mainly by autoschizis, a novel form of cell death. Basis for their potential use as adjuvants in anticancer therapy. *Eur J Med Chem* 2003;38: 451–7.
40. Gilloteaux J, Jamison JM, Neal DR, Summers JL. Xenotransplanted human prostate carcinoma (DU145) cells develop into carcinomas and cribriform carcinomas: Ultrastructural aspects. *Ultrastruct Pathol* 2012;36: 294–311.
41. Gilloteaux J, Jamison JM, McGuire K, et al. Autoschizis: A novel cell death induced in tumors by a new anticancer adjuvant or therapy. Royal Society of Medicine, Oncology Section. London Meeting on Translational Development against Cancer. 2012; 17 p. (abstract).
42. Gilloteaux J, Jamison JM, Arnold D, Summers JL. Human prostate DU145 carcinoma cells implanted in nude mice remove the peritoneal mesothelium to invade and grow as carcinomas. *Anat Rec A Disc Mol Cell Evol Biol* 2013;296: 40–55.
43. Jamison JM, Gilloteaux J, Taper HS, et al. The in vitro and in vivo antitumor activity of vitamin C: K3 combinations against prostate cancer. In: Lucas JL, ed. *Trends in prostate cancer research*. Hauppauge (NY): Nova Science, 2005:423–71.
44. Tareen B, Summers JL, Jamison JM, et al. A 12-week, open label, phase I/IIa study using Apatone® for the treatment of prostate cancer patients who have failed standard therapy. *Int J Med Sci* 2008;5: 62–7.
45. Gilloteaux J, Naud J. The zinc iodide-osmium tetroxide staining- fixative of Maillet. Nature of the precipitate studied by x-ray microanalysis and detection of Ca2+ -affinity subcellular sites in a tonic smooth muscle. *Histochemistry* 1979;63: 227–43.
46. Carruba G, Pavone C, Pavone-Macalusa M, et al. Morphometry of in vitro systems. An image analysis of two human prostate cancer cell lines (PC-3 and DU145). *Pathol Res Prac* 1989;185: 704–8.
47. Ren J. Relationship between development of microvilli on tumor cells and growth or metastatic potential of tumor cells. *Hokkaido Igaku Zasshi* 1991;66: 187–200.
48. Gonda MA, Aaronson SA, Ellmore N, et al. Ultrastructural studies of surface features of human normal and tumor cells in tissue culture by scanning and transmission electron microscopy. *J Natl Cancer Inst* 1976;56: 245–63.
49. Frost JK. The cell in health and disease. An evaluation of cellular morphologic expression of biologic behaviour, 2nd ed, revised. In: Wied JI, ed. Basel: Karger. *Monogr Clin Cytol* 1986;2: 1–304.

50. Srigley JR, Hartwick WJ. Selected ultrastructural aspects of urothelial and prostatic tumors. *Ultrastruct Pathol* 1988;12: 49–65.
51. Coene E, Van Oostveldt P, Willems K, et al. BRCA1 is localized in cytoplasmic tube-like invaginations in the nucleus. *Nat Genet* 1997;16: 122–4.
52. Burns ER, Soloff BL, Hanna C, Buxton DF. Nuclear pocket associated with the nucleolus in normal and neoplastic cells. *Cancer Res* 1971;31: 159–65.
53. Johnson N, Krebs M, Boudreau R, et al. Actin-filled nuclear invaginations indicate degree of cell de-differentiation. *Differentiation* 2003;71: 414–24.
54. Lagace TA, Ridgway ND. The rate-limiting enzyme in phosphatidylcholine synthesis regulates proliferation of the nucleoplasmic reticulum. *Mol Biol Cell* 2005;16: 1120–30.
55. Dahl KN, Ribeiro AJS, Lammerding J. Nuclear shape, mechanics, and mechanotransduction. *Circ Res* 2008;102: 1307–18.
56. Horesjsi B, Vinopal S, Stadkova V, et al. Nuclear γ-tubulin associates with nucleoli and interacts with tumor suppressor protein C53. *J Cell Physiol* 2012;227: 367–82.
57. Clubb BH, Locke M. 3T3 cells have nuclear invaginations containing F-actin. *Tissue Cell* 1998;30: 684–91.
58. Bourgeois CA, Hubert J. Spatial relationship between the nucleolus and the nuclear envelope: Structural aspects and functional significance. *Int Rev Cytol* 1988;111: 1–52.
59. Bush H, Byvoet P, Smetana K. The nucleolus of the cancer cell: A review. *Cancer Res* 1963;23: 313–39.
60. Goessens G. Nucleolar structure. *Int Rev Cytol* 1984;87: 107–58.
61. Raška I, Shaw PJ, Cmarko D. New insights into nucleolar architecture and activity. *Int Rev Cytol* 2006;255: 177–234.
62. Derenzini M, Betts CM, Ceccarelli C, Eusebi V. Ultrastructural organization of nucleoli in benign and malignant melanomas. *Virchows Arch B Cell Pathol Incl Mol Pathol* 1986;5: 342–52.
63. Kessel RG. Annulate lamellae: A last frontier in cellular organelles. *Int Rev Cytol* 1992;133: 43–120.
64. Bannash P. The cytoplasm of hepatocytes during carcinogenesis. In: Rentchnick P, ed. *Recent results in cancer research*. New York: Springer Verlag, Inc., 1968.
65. Podmore ID, Griffiths HR, Herbert KE, et al. Vitamin C exhibits pro-oxidant properties. *Nature* 1998;392: 559.
66. Gilloteaux J, Jamison JL, Neal DA, Summers JL. Cell death by autoschizis in TRAMP prostate carcinoma cells as a result of treatment by ascorbate: Menadione combination. *Ultrastruct Pathol* 2005;28: 221–36.
67. Lupulescu A. Ultrastructure and cell surface studies of cancer cells following vitamin C treatment. *Exp Toxicol Pathol* 1992;44: 3–9.
68. Koch CJ, Biaglow JE. Toxicity, radiation sensitivity modification and metabolic effects of dehydroxyascorbate and ascorbate in mammalian cells. *J Cell Physiol* 1978;94: 299–306.
69. Szent-Györgyi A. Observations on the function of peroxidase systems and the chemistry of the adrenal cortex: Description of a new carbohydrate derivative. *Biochem J* 1928;22: 1387–409.
70. Pedersen T, Aebi U. Nuclear actin extends, with no contraction in sight. *Mol Biol Cell* 2005;16: 5055–60.
71. Philomonenko W, Janácek J, Harata M, Hozák P. Transcription-dependent rearrangements of actin and nuclear myosin I in the nucleolus. *Histochem Cell Biol* 2010;134: 243–9.
72. Desai ID, Tappel AL. Damage to proteins by peroxidized lipids. *J Lipid Res* 1963;58: 204–7.
73. Maramag C, Menon M, Blaji KC, et al. Effect of vitamin C on prostate cancer cells in vitro: Effect on cell number, viability, and DNA synthesis. *Prostate* 1997;32: 188–95.
74. Orrenius S, McConkey DJ, Nicotera P. Role of calcium in toxic and programmed cell death. *Adv Exp Med Biol* 1991; 283: 419–25.
75. Farber JL, Kyle ME, Coleman JB. Mechanisms of cell injury by activating oxygen species. *Lab Invest* 1990;62: 670–9.
76. Sakagami H, Satoh K. Modulating factors of radical intensity and cytotoxic activity of ascorbate. *Anticancer Res* 1997;17: 3513–20.
77. Atkinson DE. The energy charge of the adenylate pool as a regulator parameter: Interaction with feedback modifiers. *Biochemistry* 1968;7: 4030–40.
78. Hernandez-Verdun D. Assembly and disassembly of the nucleolus during the cell cycle. *Nucleus* 2011;2: 189–94.
79. Jamison JM, Gilloteaux J, Koch JA, et al. Vitamin C and K_3-induced oxidative stress in human prostate tumor cells: Mitochondrial ultrastructural alterations. *Microsc Microanal* 1997;3: 23–4.
80. Tardy C, Codogno P, Autefage H, et al. Lysosomes and lysosomal proteins in cancer cell death (new Players of an old struggle). *Biochim Biophys Acta* 2006;1765: 101–25.
81. McGuire K, Jamison JM, Neal D, et al. Elucidating the pathway of Apatone® induced DNase II reactivation during autoschizic cell death. *Microsc Microanal* 2009;15: 888–9.
82. Wu FY, Chang NT, Chen WJ, Juan CC. Vitamin K3-induced cell cycle arrest and apoptotic cell death are accompanied by altered expression of *c-fos* and *c-myc* in nasopharyngeal carcinoma cells. *Oncogene* 1993;8: 2237–44.
83. Wu FY, Liao WC, Chang HM. Comparison of antitumor activity of vitamins K1, K2 and K3 on human tumor cells by two (MTT and SRB) cell viability assays. *Life Sci* 1993;52: 1797–804.
84. Ngo E, Sun TP, Chang JY, et al. Menadione-induced damage in a human tumor cell line. *Biochem Pharmacol* 1991;41: 1283–92.
85. Dypbukt JM, Ankerona M, Burkitt M, et al. Different peroxidant levels stimulate growth, trigger apoptosis, or produce necrosis of insulin-secreting RINm5F cells. *J Biol Chem* 1997;269: 30553–60.
86. Markovits J, Sun TP, Juan CC, et al. Menadione (vitamin K_3) enhances the mitogenic signal of epidermal growth factor via extracellular signal-regulated kinases. *Int J Oncol* 1998;13: 1163–70.
87. Bellomo G, Mirabelli F, Vairetti M, et al. Cytoskeleton as target in menadione-induced oxidative stress in cultured mammalian cells. Biochemical and immunocytochemical features. *J Cell Physiol* 1998;143: 118–28.
88. Napirei M, Wulf S, Mannherz HG. Chromatin breakdown during necrosis by serum Dnase1 and the plasminogen system. *Arthritis Rheum* 2004;50: 1873–83.
89. Gerasimenko JV, Gerasimenko OV, Palejwala A, et al. Menadione-induced apoptosis: Roles of cytosolic Ca2+ elevations and the mitochondrial permeabilityu transition pore. *J Cell Sci* 2001;115: 485–97.
90. Osada S, Sakashima F, Hosona Y, et al. Extracellular signal-regulated kinase phosphorylation due to menadione-induced arylation mediates growth inhibition of pancreas cancer cells. *Cancer Chemother Pharmacol* 2008;62: 315–20.
91. Di Monte D, Bellomo G, Thor H, et al. Menadione-induced cytotoxicity is associated with protein thiol oxidation and alteration in intracellular Ca2+ homeostasis. *Arch Biochem Biophys* 1984;235: 343–50.
92. Scott GK, Atsriku C, Kaminker P, et al. Vitamin K3 (menadione)-induced oncosis associated with keratin 8 phosphorylation and histone H3 arylation. *Mol Pharmacol* 2005;68: 606–15.
93. Townsend DM, Tew KD, Tapiero H. The importance of glutathione in human disease. *Biomed Pharmacother* 2003; 57: 145–55.

94. Arrick BA, Griffith OW, Cohn ZA. Glutathione depletion sensitizes tumor cells to oxidative cytolysis. *J Biol Chem* 1982;257: 1231–7.
95. Rando OJ, Zhao K, Crabtree GR. Searching for a function for nuclear actin. *Trends Cell Biol* 2000;10: 92–7.
96. Rando OJ, Zhao K, Janmey P, Crabtree GR. Phosphatidylinositol-dependent actin filament binding by the SWI/SNF-like BAF chromatin remodelling complex. *Proc Natl Acad Sci USA* 2002;99: 2824–9.
97. Spencer VA, Costes S, Inman JL, et al. Depletion of nuclear actin is a key mediator of quiescence in epithelial cells. *J Cell Sci* 2011;24: 123–32.
98. Thériot JA, Mitchison TJ. Actin microfilament dynamics in locomoting cells. *Nature* 1991;352: 126–31.
99. Akman SA, Dietrich M, Chlebowski R, et al. Modulation of cytotoxicity of menadione sodium bisulfite versus leukemia L1210 by the acid-soluble thiol pool. *Cancer Res* 1985;45: 5257–62.
100. Carbonera D, Azzone GF. Permeability of inner mitochondrial membrane and oxidative stress. *Biochim Biophys Acta* 1988;943: 245–55.
101. Gilloteaux J, Eze N, Jamison JM, et al. A rare, human prostate oncocyte cell originates from the prostatic carcinoma (DU145) cell line. *Ultrastruct Pathol* 2013;37: 1–9.
102. Kabsch W, Mannherz HG, Suck D. Three-dimensional structure of the complex of actin and DNAse I at 4.5 Å resolution. *EMBO J* 1985;4: 2113–18.
103. Kabsch W, Mannherz HG, Suck D, et al. Atomic structure of the actin: DNase I complex. *Nature* 1990;347: 37–44.
104. Malorni W, Iosi F, Mirabelli F, Bellomo G. Cytoskeleton as a target in menadione-induced oxidative stress in cultured mammalian cells: Alterations underlying surface bleb formation. *Cell Biol Interact* 1991;80: 217–36.
105. Burtnick LD, Chan KW. Deoxyribonuclease I binding masks the major tryptic cleavage sites of actin. *Life Sci* 1980;26: 1323–7.
106. Thiry M. DNase I-sensitive sites within the nuclear architecture visualized by immunoelectron microscopy. *DNA Cell Biol* 1991;10: 169–80.
107. Kerr JF, Wyllie AH, Currie AR. Apoptosis: A basic biological phenomenon with wide-ranging implications in tissue kinetics. *Br J Cancer* 1972;26: 239–57.
108. Gewies A, Rocklin OW, Cohen MB. Ceramide induces cell death in the human prostatic carcinoma cell lines PC3 and DU145 but does not seem to be involved in Fas-mediated apoptosis. *Lab Invest* 2000;80: 671–6.
109. Franke WW, Kartenbeck J. Outer mitochondrial membrane continuous with endoplasmic reticulum. *Protoplasma* 1971;73: 35–41.
110. Baumgartner HK, Gerasimenko JV, Thorne C, et al. Calcium elevation in mitochondria is the main Ca^{2+} requirement for mitochondrial permeability transition pore (mPTP) opening. *J Biol Chem* 2009;284: 20796–803.
111. Criddle DN, Gillies S, Baumgartner-Wilson HK, et al. Menadione-induced reactive oxygen species generation via redox cycling promotes apoptosis of murine pancreastic acinar cells. *J Biol Chem* 2006;281: 40485–92.
112. Melgar ML, Anadon A, Bello J. Effects of menadione on the cardiovascular system. *Vet Hum Toxicol* 1991;33: 110–14.
113. Hamasaki M, Furuta N, Matsuda A, et al. Autophagosomes form at ER-mitochondria contact sites. *Nature* 2013;495: 389–93.
114. Hallman A, Milczarek R, Lippinski M, et al. Fast perinuclear clustering of mitochondria in oxidatively stressed human choriocarcinoma cells. *Folia Morphol* 2004;63: 407–12.
115. Noto V, Taper HS, Jiang YH, et al. Effects of sodium ascorbate (vitamin C) and 2-methyl-1,4-naphtoquinone (vitamin K3) treatment on human tumor cell growth in vitro. I. Synergism of combined vitamin C and K3 action. *Cancer* 1989;63: 901–6.
116. Von Gruenigen VE, Jamison JM, et al. The *in vitro* antitumor activity of vitamins C and K_3 against ovarian carcinoma. *Anticancer Res* 2003;23: 3279–87.
117. Bonilla-Porras AR, Jimenez-Del Rio M, Velez-Pardo C. Vitamin K3 and vitamin C alone or in combination induced apoptosis in leukemia cells by a similar oxidative stress signalling mechanism. *Cancer Cell Int* 2011;11: 19.
118. Warburg O, Wind F, Negelein E. The metabolism of tumors in the body. *J Gen Physiol* 1927;8: 519–30.
119. Warburg O. On respiratory impairment in cancer cells. *Science* 1956;124: 369–70.
120. Bernhard W. Drug-induced changes in the interphase nucleus. *Adv Cytopharmacol* 1971;1: 49–67.
121. Simard R. The nucleus: Action of chemical and physical agents. *Int Rev Cytol* 1970;28: 169–211.
122. Simard R, Bernhard W. Le phénomène de la ségrégation nucléolaire: Spécificité d'action de certains antimétabolites. *Int J Cancer* 1966;1: 463–79.
123. Smetana K, Potměsil M. Ring shaped nucleoli in liver cells of rats after treatment with actinomycin D. *Z Zellforsch Mikrosk Anat* 1968;92: 62–9.
124. Bassleer R, Goessens G, Lepoint A, et al. Contribution à l'étude des effets d'agents antimitotiques sur des cellules animales normales ou ancéreuses. Analyses cytologiques et cytochimiques quantitatives. *Bull Mém Acad Roy Med Belg* 1967;13: 496–502.
125. Daoust R, Amano H. Ribonuclease and deoxiribonuclease activities in experimental and human tumors by the histochemical substrate film method. *Cancer Res* 1963;23: 131–4.
126. Chobert MN, Pouchelet M, Anteunis A, et al. Nucleolar lesions induced by ribonuclease in living cultured cells. *Biol Cell* 1983;49: 19–28.
127. Cogliati R, Gautier A. Demonstration of DNA and polysaccharides using a new ''Schiff type'' reagent. *C R Acad Sci Hebd Séances Acad Sci D* 1973;276: 3041–4.
128. Smetana K, Busch H. Studies on the ultrastructure of the nucleoli of the Walker tumor and rat liver. *Cancer Res* 1964;24: 537–57.
129. Ervin E, Jamison JM, Gilloteaux J, et al. Characterization of the early events in vitamin C and K3-induced death of human bladder tumor cells. *Scanning* 1998;20: 210–11.
130. Monneron A, Bernhard W. Fine structural organization of the interphase nucleus in some mammalian cells. *J Ultrastruct Res* 1969;27: 266–88.
131. Moyne G. Feulgen-derived techniques for electron microscopical cytochemistry of DNA. *J Ultrastruct Res* 1973;45: 102–23.
132. Fakan S, Puvion E. The ultrastructural visualization of nucleolar and extranucleolar RNA synthesis and distribution. *Int Rev Cytol* 1980;65: 255–99.
133. Saitoh N, Spahr CS, Patterson SD, et al. Proteomic analysis of interchromatin granule clusters. *Mol Biol Cell* 2004;15: 3876–90.
134. Fraschini A, Albi E, Gahan PB, Viola-Magni MP. TEM cytochemical study of the localization of phospholipids in interphase chromatin in rat hepatocytes. *Histochemistry* 1992;97: 225–35.
135. Wassef M. A cytochemical study of interchromatin granules. *J Ultrastruct Res* 1979;69: 121–33.
136. Johnston JA, Ward CL, Kopito RR. Aggresomes: A cellular response to misfolded proteins. *J Cell Biol* 1990;143: 1883–98.

137. Johnston JA, Illing ME, Kopito RR. Cytoplasmic dynein/dynactin mediates the assembly of aggresomes. *Cell Motil Cytoskeleton* 2002;53: 26–38.
138. Gilloteaux J, Jennes L, Stoeckel ME, Vanderhaeghen J-J. Focal ellipsoid deposits in the atrial myocytes of Syrian hamster. *Ultrastruct Pathol* 1994;18: 221–7.
139. Wyllie AH. Apoptosis: An overview. *Brit Med Bull* 1997; 53: 451–65.
140. Falcieri E, Gobbi P, Zamai L, Vitale M. Ultarstructural features of apoptosis. *Scanning Microsc Intl* 1994a;8: 653–66.
141. Saraste A. Morphologic criteria and detection of apoptosis. *Herz* 1999;24: 189–95.
142. Biggiogera M, Bottone MG, Pelliciari C. Nuclear RNA is extruded from apoptotic cells. *J Histochem Cytochem* 1998; 46: 999–1005.
143. Majno G, Joris I. Apoptosis, oncosis, and necrosis. An overview of cell death. Fine structural organization of the interphase nucleus in some mammalian cells. *J Ultrastruct Res* 1995;27: 266–88.
144. Deter RL, Baudhuin P, De Duve C. Participation of lysosomes in cellular autophagy induced in rat liver by glucagon. *J Cell Biol* 1967;35: C11–16.
145. Ericsson JLE. Mechanism of cellular autophagy. In: Dingle JT, Fell HB, eds. *Lysosomes in biology and pathology.* Amsterdam: North-Holland Publishing Co, 1969;345–94.
146. Allison AC. Lysosomes and cancer. In: Dingle JT, Fell HB, eds. *Lysosomes in biology and pathology.* Amsterdam: North Holland Publ Co., 1990;178–204.
147. Levine B, Yuan J. Autophagy in cell death: An innocent convict? *J Clin Invest* 2005;115: 2679–88.
148. Wyllie AH, Beattie GJ, Hargreaves AD. Chromatin changes in apoptosis. *Histochem J* 1981;13: 681–92.
149. Arends MJ, Morris RG, Wyllie AH. Apoptosis. The role of the endonuclease. *Am J Pathol* 1990;136: 593–608.
150. Walker NI, Harmon BV, Gobé GC, Kerr JF. Patterns of cell death. *Methods Achiev Exp Pathol* 1988;13: 18–54.
151. Velkey JM, Bernanke DH. Apoptosis during coronary artery orifice development in the chick embryo. *Anat Rec* 2001;262: 310–17.
152. Tavassoli M, Crosby WH. Fate of the nucleus of the marrow erythroblast. *Science* 1973;179: 912–13.
153. Sonoda Y, Sasaki K, Suda M, et al. Effects of colchicine on the enucleation of erythroid cells and macrophages in the liver of mouse embryos: Ultrastructural and three-dimensional studies. *Anat Rec* 1998;251: 290–6.
154. Aumüller G, Seitz J, Riva A. Functional morphology of prostate gland. In: Riva A, Testa-Riva F, Motta PM, eds. *Ultrastructure of male urogenital glands*. Boston (MA): Kluwer Acad, 1994;61–112.
155. Kudo S. Differentiation of Clara cells and pneumocytes of the rat by means of enzyme- and immunohistochemistry. *Anat Rec* 1994;238: 49–56.